(1)

FR-60298

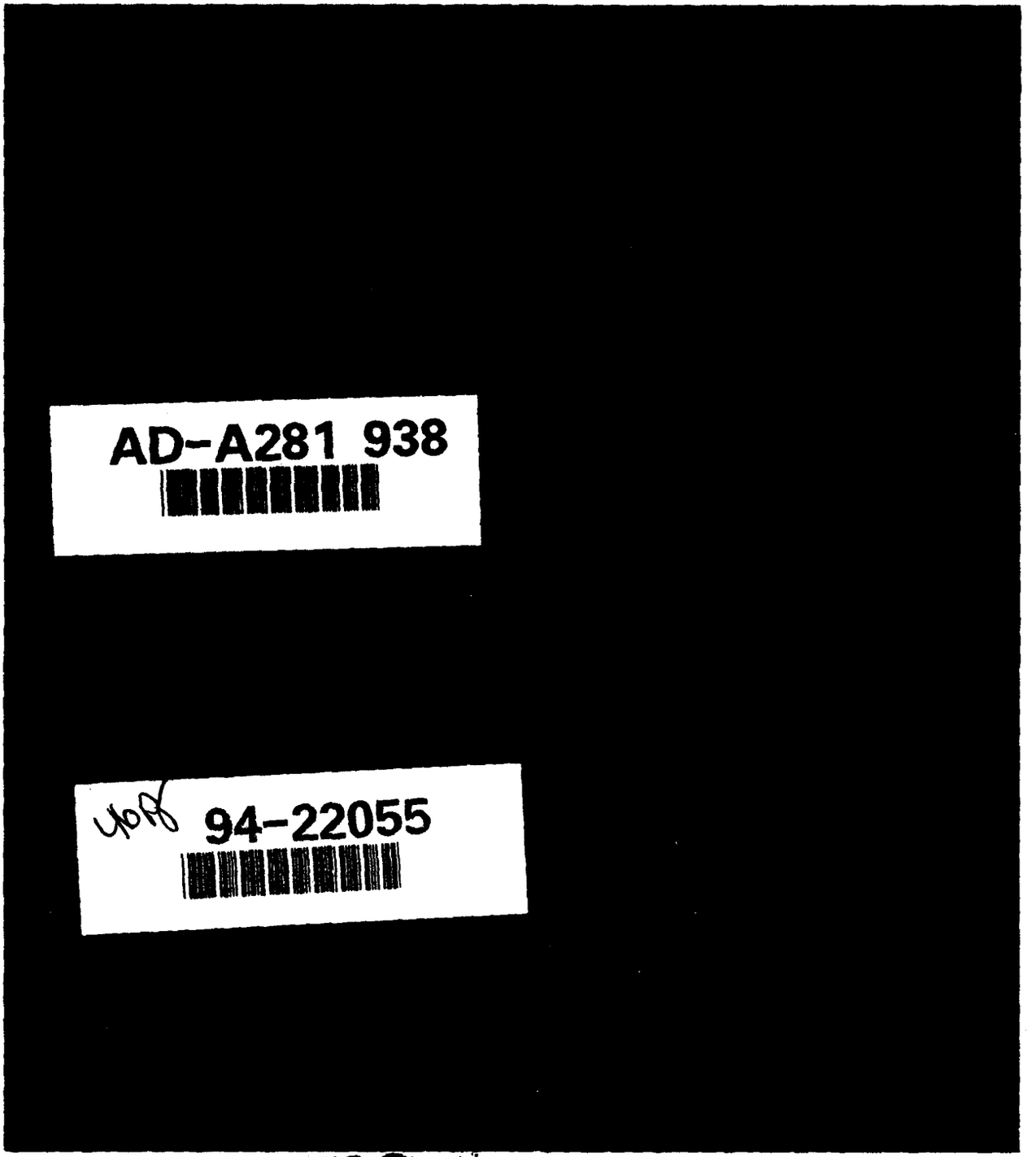

spire

Spire Corporation/One Patriots Park/Bedford, MA 01730-2396

DISCLAIMER NOTICE

THIS DOCUMENT IS BEST QUALITY AVAILABLE. THE COPY FURNISHED TO DTIC CONTAINED A SIGNIFICANT NUMBER OF COLOR PAGES WHICH DO NOT REPRODUCE LEGIBLY ON BLACK AND WHITE MICROFICHE.

FR-60298

A Final Report for:

SILICON-BASED BLUE LIGHT EMITTING DIODE

Submitted under:

Contract Number N00014-93-C-0176

Funded by:

Ballistic Missile Defense Organization

Covering period:

1 January through 28 February 1994

Submitted to:

Scientific Officer, NCCOSC RDTE DIV (NRaD)

53570 Silvergate Avenue

San Diego, CA 92152-5070

Submitted by:

Spire Corporation

One Patriots Park

Bedford, MA 01730-2396

REPORT DOCUMENTATION PAGE

Form Approved
OMB No. 0704-0188

1. AGENCY USE ONLY *(Leave blank)*	2. REPORT DATE	3. REPORT TYPE AND DATES COVERED
	27 May 1994	Final Technical, 1JAN-28FEB94

4. TITLE AND SUBTITLE

Silicon-based Blue Light Emitting Diode

5. FUNDING NUMBERS

N00014-93-C-0176

6. AUTHOR(S)

Fereydoon Namavar

7. PERFORMING ORGANIZATION NAME(S) AND ADDRESS(ES)

Spire Corporation
One Patriots Park
Bedford, MA 01730-2396

8. PERFORMING ORGANIZATION REPORT NUMBER

FR-60298

9. SPONSORING/MONITORING AGENCY NAME(S) AND ADDRESS(ES)

Ballistic Missile Defense Organization
7100 Defense Pentagon
Washington, DC 20301-7100

Office of Naval Research
53570 Silvergate Avenue
San Diego, CA 92152-5070

10. SPONSORING/MONITORING AGENCY REPORT NUMBER

11. SUPPLEMENTARY NOTES

12a. DISTRIBUTION/AVAILABILITY STATEMENT

12b. DISTRIBUTION CODE

13. ABSTRACT *(Maximum 200 words)*

Phase I results demonstrated for the first time a strong, stable blue-green emission from C-implanted red-emitting porous silicon. The objective of Phase I was to obtain blue-green emission from porous Si structures either by increasing the bandgap of the substrate by growth of Si-C random alloys prior to forming nanostructures with quantum confined properties, or by increasing the confinement energy of red-emitting Si nanostructures.

Porous structures fabricated from group IV alloys epitaxially grown by chemical vapor deposition (CVD) resulted in an enhancement in light emission of about one order of magnitude after incorporation of a very small amount of carbon in the epitaxial grown films. Strong blue-green light emission was observed by the naked eye from C-implanted and annealed porous Si. Using AlGaAs as a reference, we observed that the intensity of blue-green emission was one order of magnitude higher than that of the original red-emitting porous Si. Catholuminescence measurements of our samples performed at the University of Colorado show blue emission at 1.80 eV and 2.80 eV. Fourier transform infrared (FTIR) spectra of a blue-green emitting porous structure shows an IR absorption line identical to that of SiC and electron diffraction studies clearly show reflections corresponding to β-SiC.

Phase I results indicate that blue-green light is from SiC nanostructures with quantum confined properties. This material may be used to fabricate blue light-emitting Si-based devices which can be easily integrated into Si technology.

14. SUBJECT TERMS

Red-emitting Porous Si, Carbon Implantation, SiC Nanostructures, Bandgap Engineering, Blue-green Emission, Epitaxial Si-C

15. NUMBER OF PAGES

37

16. PRICE CODE

17. SECURITY CLASSIFICATION OF REPORT	18. SECURITY CLASSIFICATION OF THIS PAGE	19. SECURITY CLASSIFICATION OF ABSTRACT	20. LIMITATION OF ABSTRACT
UNCLASSIFIED	UNCLASSIFIED	UNCLASSIFIED	UNLIMITED

TABLE OF CONTENTS

LIST OF FIGURES

LIST OF FIGURES (Continued)

LIST OF FIGURES (Concluded)

LIST OF TABLES

1 INTRODUCTION

Although junction devices in crystalline silicon have excellent properties for use as electronic amplifiers and switches, silicon is not recognized as a premier material based on its optoelectronic properties. In general, silicon's optical properties are severely compromised, because the material possesses an indirect optical bandgap. Basically, in order for an electron in the excited state (conduction band) of silicon to recombine into the ground state (valence band) while generating radiative emission, a third body, *viz.*, a phonon, must be involved, and such three-body processes have very low probability. Thus, although photoluminescence (PL) in the near infrared (IR) at 1.1 eV (1100 nm) can be observed in standard bulk Si samples, it is extremely weak.[1] In fact, the external quantum efficiency of forward bias electroluminescence (EL) at 1100 nm in conventional diffused crystalline Si np junctions is less than 10^{-4}%, basically the result of the indirect bandgap.[2] In contrast, the external quantum efficiency of direct bandgap GaAs light-emitting diodes (LEDs) certainly exceeds 1%,[3] while the internal quantum efficiency may be as high as 80%.[4]

It was recently reported that highly-efficient, optically-excited, visible light emission (PL) is indeed possible from silicon[5] if the material is properly prepared in a nanostructural form, typically by electrochemical and/or chemical etching.[6] As a direct consequence of the etch procedure, the porous Si is composed of a sponge-like network of channels, which support a myriad of microscopic wire-like protuberances located all over the internal surfaces of the pores. High magnification transmission electron microscopy (TEM) appears to confirm the presence of these basically one-dimensional structures, 10 nm or less in diameter.[7] Such nanostructures exhibit quantum confinement effects, leading to a large increase in the effective energy gap.[8] In fact, the absorption edge, for such "wires" with roughly a 20Å diameter, was shown to be shifted to a wavelength of about 550 nm which is in the yellow-green part of the visible spectrum.[9]

At Spire we have fabricated porous Si samples on standard p-type crystalline Si substrates by electrochemical means, then tested their properties under optical excitation, and studied the effects of alloying with germanium. This effort has proven to be extremely productive: very significantly intense PL emission peaks throughout the visible and near IR spectral regions were demonstrated, and the properties of the peaks were studied over a temperature range from 4 to 700K.[10] PL excitation spectra were also determined, as was the dependence of PL intensity on excitation intensity. The addition of Ge was shown to cause a red-shift in the emission wavelength. Figure 1 compares PL results from a porous structure on pure Si with a porous structure produced on an epitaxial SiGe film 10 μm thick with a concentration of 6% Ge, clearly showing a red shift from 689 nm to 725 nm. Note that the etching process was carried out under similar conditions for both samples.

Figure 2 shows PL spectra of several porous Si samples fabricated in our laboratory under different conditions of chemical etching, chosen to provide different wire diameters. Asymmetries in some curves are an artifact from an optical filter with cutoff characteristics at 520 nm, which was required to eliminate any phonons emitted directly from the laser from entering the field of the detector. These red, orange, yellow and green colors could be clearly identified either on a series of samples prepared separately under different conditions, or spatially separated across the surface of a sample processed with graded properties. Longer etch periods

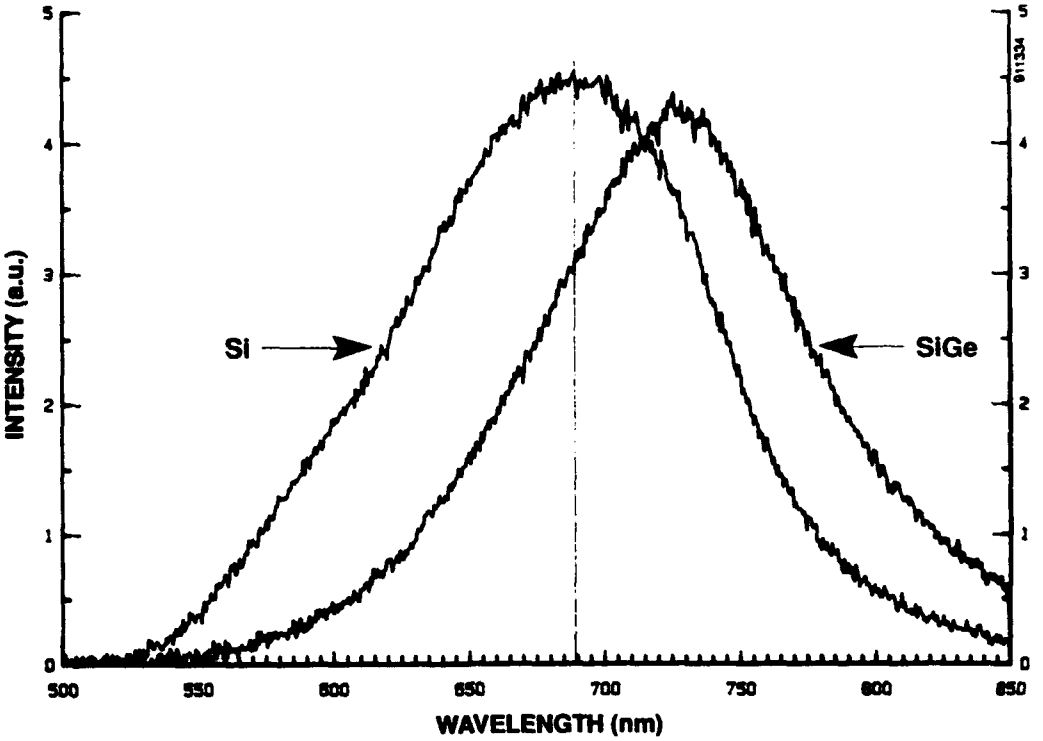

Figure 1 *Comparison of PL from porous Si and a porous structure produced on an epitaxial SiGe film with a 6% Ge concentration.*

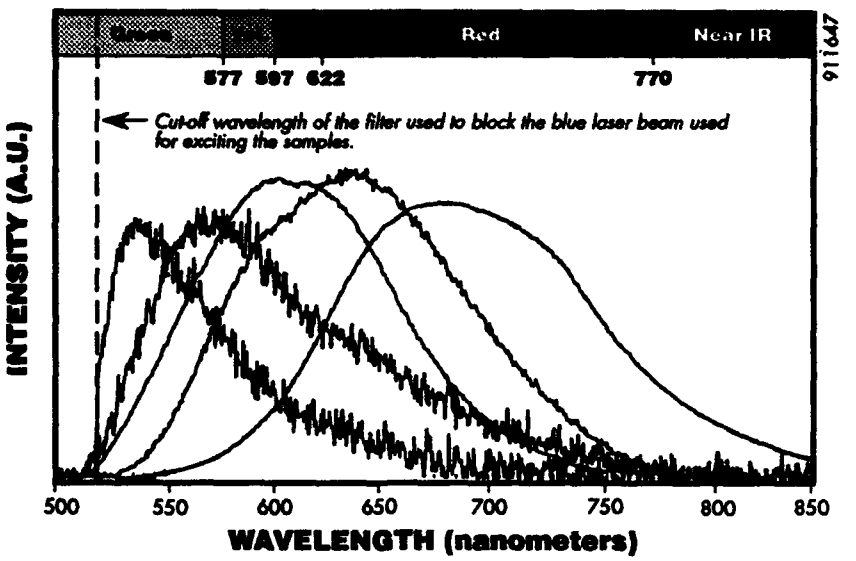

Figure 2 *PL spectra of several porous Si samples; excitation obtained with an argon laser emitting at 488 nm. Note that emission at shorter wavelengths is weaker and more unstable over time.*

always resulted in smaller Si nanostructures. However, based on our results, the Si crystallites with light emission below yellow wavelengths are physically too fragile and unstable even over short periods of time, therefore they are not useful for device fabrication.

Spire was the first to fabricate yellow- and orange-emitting heterojunction LEDs based on silicon, as shown in Figure 3.[11,12] These devices, which operated in air at room temperature, were fabricated by depositing a wide bandgap n-type semiconductor (indium-tin-oxide [ITO]) onto the surface of a p-type silicon wafer which had been electrochemically etched to produce a porous layer with nanometer-sized Si crystallites. Other researchers have used semi-transparent Au as a solid state contact to porous Si to form Schottky diodes.[13,14] However, the use of ITO or other wide bandgap semiconductors[15] (see Table I) which are transparent to visible light has potential for visible LEDs and display panels. The results from Spire have achieved nationwide media attention through reports in a number of magazines and newspapers including the Wall Street Journal(December 6, 1991, p. B3), Scientific American (March 1992, p. 102), Lasers & Optronics (January 1992 , Vol. No. 1, p. 8), the Electronics Engineering Time (May 25, 1992, p.4), and etc.

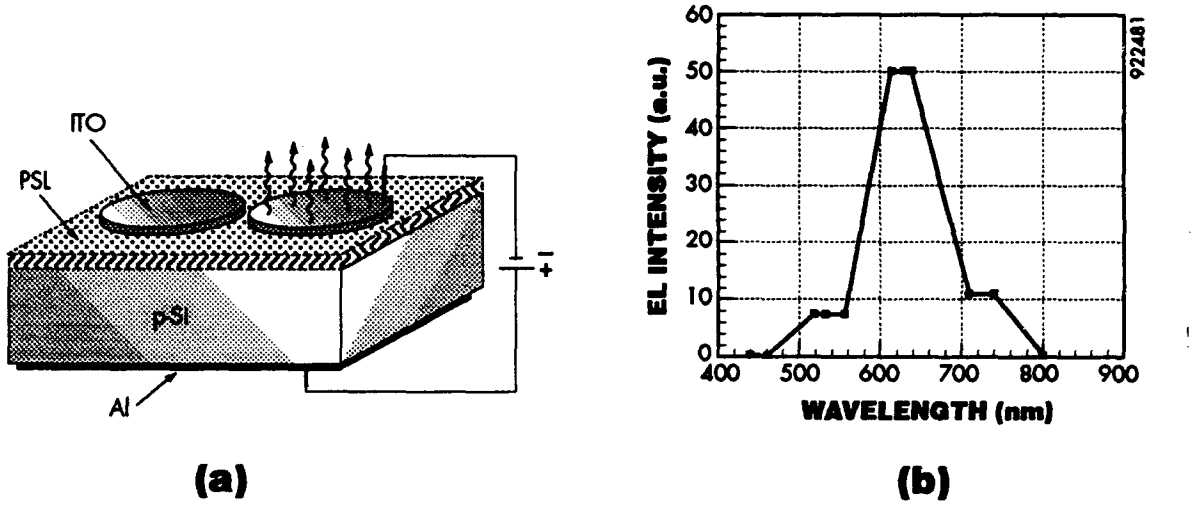

Figure 3 *An np heterojunction porous silicon LED, capable of emitting light at visible wavelengths; a) schematic cross section and b) EL spectrum.*[11]

Porous Si opens up exciting possibilities for creating optical devices in silicon and integrating electrical and optical devices with Si-based circuits. Figure 4 shows a linear dependence of light intensity on applied currents with higher levels of bias measured from a silicon-based LED. The latter and other results[12,16,17,18] indicate that observed EL originates from a minority (electron) carrier injection mechanism and demonstrate that Si-based LEDs have the same basic operating mechanism as standard commercial III-V compound-based (such as GaAs) LEDs or other homojunction devices. Figure 5 shows an energy band diagram model for ITO/porous-Si LEDs fabricated at Spire. Our results suggest that the emission efficiency of Si-based LEDs can be as impressive as the PL efficiency already observed from porous silicon. No physical or fundamental principles have been observed which would otherwise limit the emission efficiency of these devices. We believe that, by improving the materials quality and optimizing the processing parameters, devices with very high EL efficiency can be demonstrated.

Table I *List of transparent semiconductors for porous Si-based LEDS, based on Spire's patent.*[15]

P-type Materials			N-type Materials
B-doped	Mg-doped	N-doped	
C (diamond)	GaN	ZnSe	AlP
	GaP	ZnTe	GaP
	AlP	$CuAlS_2$	ZnS
	SiC	$CuAlS_2$	ZnSe
	Amorphous Si	$CuAlSe_2$	CdS
	Amorphous SiC	$CuGaS_2$	$ZnSiP_2$
		$ZnGeP_2$	$CdSiP_2$
			In_2O_3
			SnO_2
			ITO (In_2O_3 + SnO_2)
			ZnO
			CdO
			Cd_2SnO_4
			GaInN
			GaN
			SiC
			Amorphous Si
			Amorphous SiC

94778

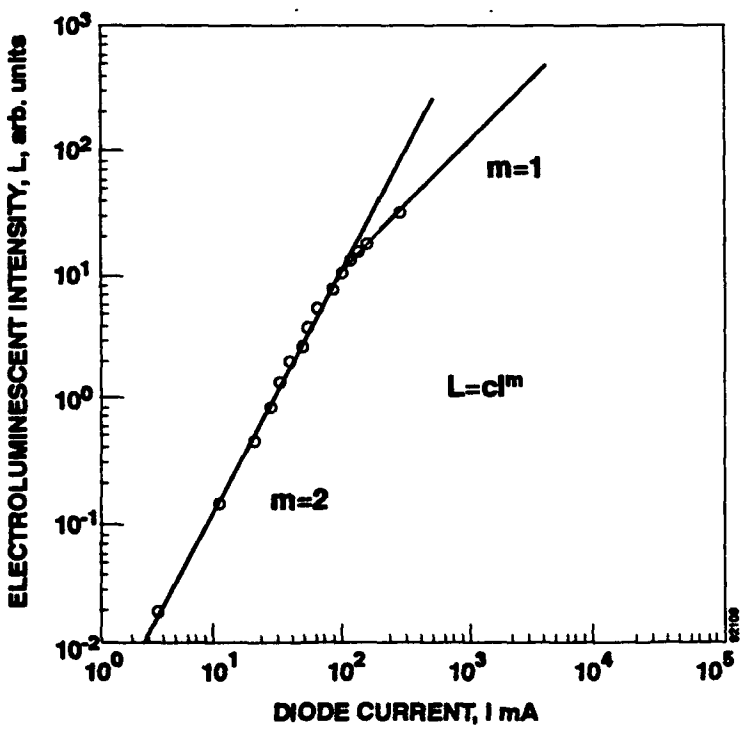

Figure 4 *Dependence of porous Si LED electroluminescence intensity on device current.*

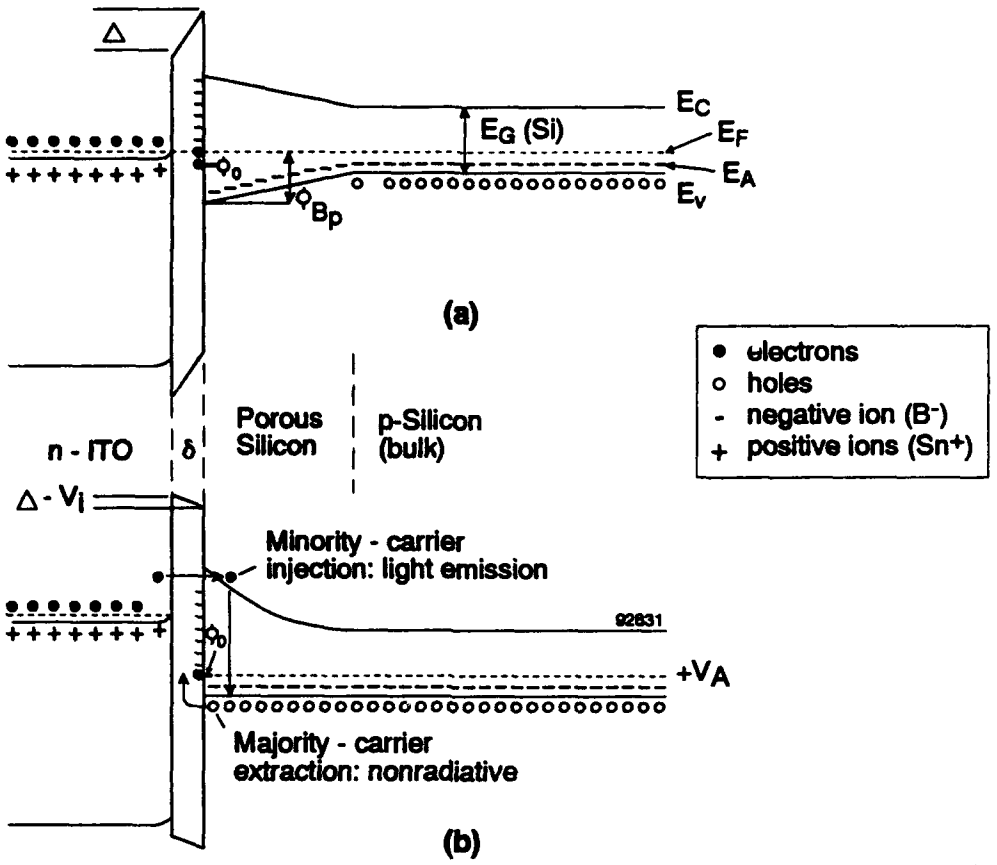

Figure 5 *Proposed energy band diagram model for ITO/porous Si heterojunction LEDs: a) in equilibrium and b) under forward bias.*

1.1 Si Nanostructures in Porous Si Light-Emitting Devices

Using high-resolution cross-sectional transmission electron microscopy (HR-XTEM) and electron diffraction of an operational LED, we have shown the presence of nanostructures within the quantum-confinement regime.[19] Figure 6a shows an XTEM of the actual working device. The dark layer on top is the ITO which does not thin as readily as the silicon underneath it. The ITO layer has remained electron-opaque in this particular area of the sample. In other areas of the sample, where the ITO is electron-transparent, we were able to distinguish its internal microstructure. The layer below the ITO layer is porous silicon material which consists of two distinct regions. Adjacent to the ITO exists a layer approximately 1000Å thick, composed primarily of vertical pores perpendicular to the original sample surface. The remaining porous Si material beneath this layer consists of an amorphous structure with Si nanocrystals embedded within it.

Figure 6b shows a high magnification lattice image of the porous Si layer. The background microstructure is primarily amorphous; however, embedded within this amorphous material are a number of very obvious "dark spots." These dark spots are small single-crystal silicon particles with average diameters of approximately 20 to 50Å, dimensions well within the quantum confinement size regime. Note that all of the particles are still aligned with the Si substrate.

a.)

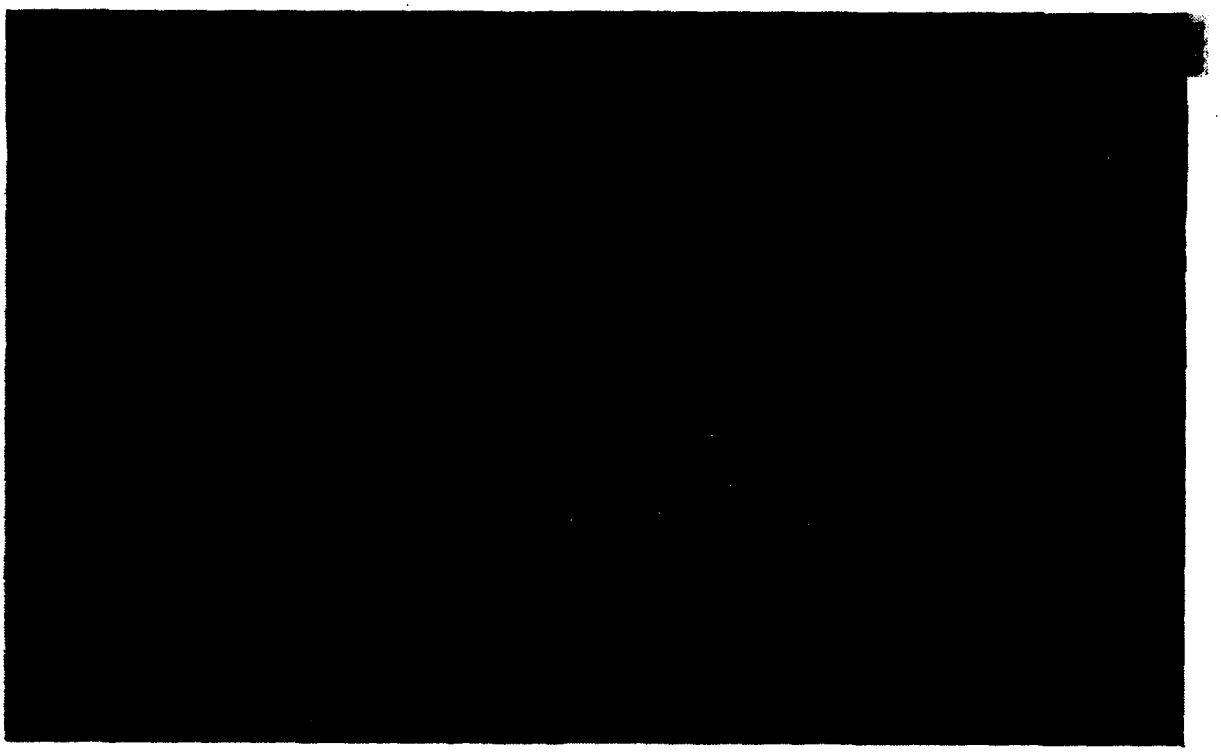

b.)

Figure 6 *A working np-heterojunction porous silicon LED, a) XTEM of the device, and b) lattice image from the porous Si region showing cross-sections of the structures with dimensions of 2, 3 and 4 nm.*[19]

1.2 Processing of Wafer-Scale Integration of Porous Si Devices

Spire has successfully developed a series of conventional bulk Si-based photolithographic processing steps to pattern selected device regions, both before and after the formation of porous Si layers.[20] Pattern resolutions better than 5 μm have been achieved. Our results indicate that pattern resolution can be significantly improved using a multiple (rather than standard single) photoresist coating process for patterning. This approach reduces the probability of cracks or pinholes which can result in the etching of undesired regions on the sample during dynamic anodic etching in the HF electrolyte. In addition we have also found that pattern resolution can be linearly improved by lowering the applied current density and shortening the etch period. We have also demonstrated the first monolithic processing of a visible LED and a photodetector on a single silicon wafer,[20] *e.g.*, true wafer-scale integration. ITO/Si np heterojunction photodiodes (or photovoltaic cells) and ITO/porous Si LEDs were fabricated monolithically on the same silicon wafer, and tested for their photovoltaic and electroluminescence properties, respectively.

1.3 Visible-light-emitting Porous Polycrystalline on Glass Substrates

The formation of Si-based light-emitting elements on a transparent substrate such as quartz or glass has great potential for the fabrication of low-cost, low-power, high-resolution thin film electroluminescent, cathodoluminescent, or plasma-induced photoluminescent displays. Recently we demonstrated[21] visible-light emission from porous structures formed in bulk and thin film polycrystalline silicon materials by anodic etching and stain etching. Figure 7 shows the PL spectrum from a thin film of PPSI-on-quartz irradiated and measured from the front side (polycrystalline silicon) and the back side of the sample.

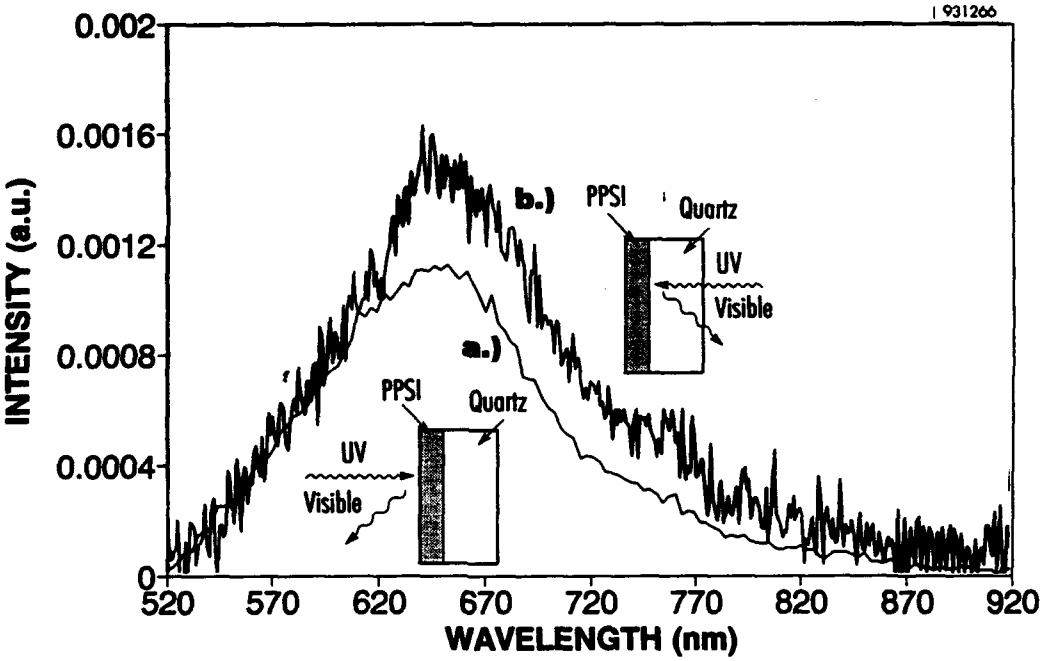

Figure 7 *PL spectrum from thin film of PPSI on quartz: (a) irradiated and measured from the front of the sample and (b) irradiated from the back of the sample with light emitted through the quartz layer.*[21]

2 PHASE I OBJECTIVE

The Phase I objective was to demonstrate blue-green photoluminescence from nanostructures of Si alloyed with carbon and germanium. The presence of Ge (lattice constant of 5.65Å) in Si-C random alloy layers on a Si substrate, is believed to relieve strain resulting from smaller atoms such as carbon (lattice constant of 3.6Å).

Why a Stable Blue-green Emission from Porous Si is Hard to Achieve - One of the major factors presently preventing the realization of stable blue-green light-emitting devices using porous Si material is the required limitation of the physical size of the Si nanostructures necessary to expand the bandgap into the blue wavelength range as shown in Figure 8.[22] The blue-green emitting crystallites formed in porous Si are presently too fragile and unacceptably susceptible to environmental effects during the processing steps required to fabricate material. The constraints on microcrystalline dimensions for producing blue LEDs can be relaxed by creating alloys of Si which intrinsically possess larger energy gaps.

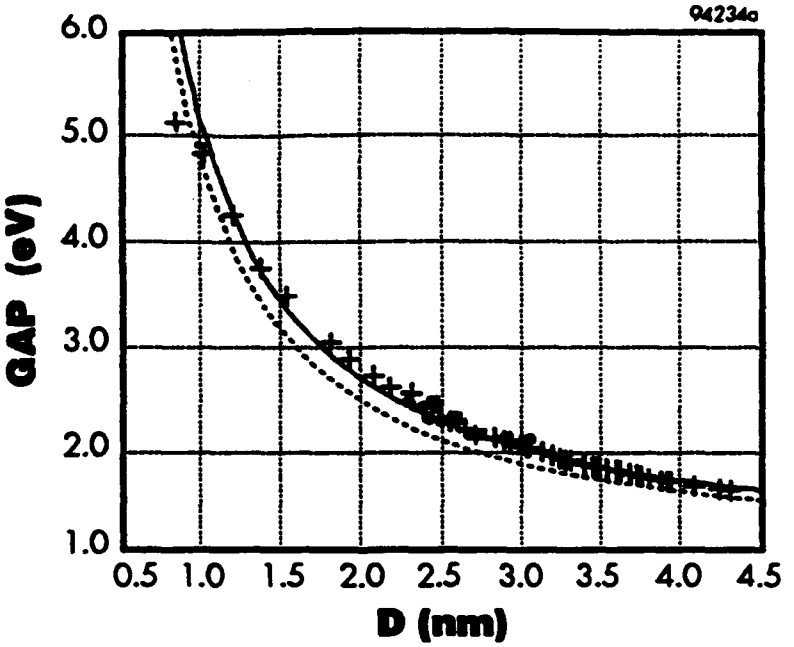

Figure 8 *Calculated bandgap energies for various silicon crystallites with respect to their diameter.*[22]

Method to Obtain Stable Blue-green Emission - We believed that blue-green emission may be obtained by: a) increasing the base bandgap of the bulk material using chemical vapor deposition (CVD) of SiC and/or SiCGe layers prior to forming quantum-sized structures. The initial increase in the bandgap of the pre-etched wafer would permit larger "quantum wires" or nanostructures to yield the energy gap required for blue- or green-emitting crystallites, or b) creating a SiC (SiGeC) phase by carbon (or C and Ge) **implantation** into red-emitting Si (and/or GeSi) nanostructures. This idea was a completely new concept that was developed recently as a result of an AF SBIR program which successfully demonstrated strong IR (1.54 μm) emission from Er-implanted Si nanostructures. These approaches are summarized in Figure 9.

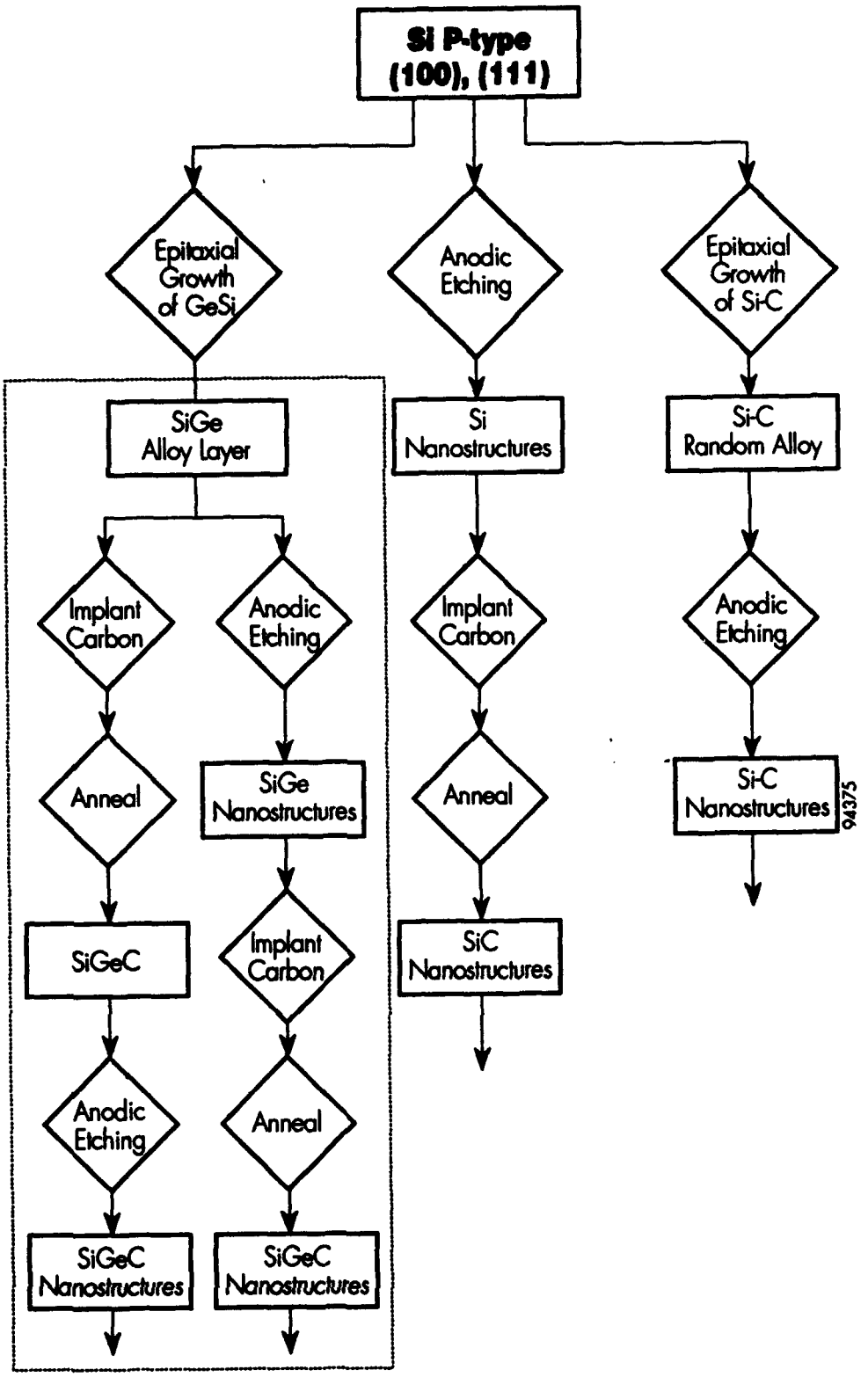

Figure 9 *Flowchart of approaches used to achieve blue-green emission from porous Si.*

3 EXPERIMENTAL PROCEDURE

3.1 CVD Growth of Epitaxial Group IV alloy layers

Si-C alloy layers were grown using an in-house AMC 7600 CVD reactor with methane (CH_4) and trichlorosilane ($HSiCl_3$) as source gases. Figure 10 shows a photograph of Spire's AMC 7600 CVD reactor. Epitaxial SiC layers about 10 μm thick were grown on p-type <111> Si wafers using various methane flow rates. The materials were grown in a temperature range of 1053°C to 1120°C.

Figure 10 *Spire's Applied Materials 7600 CVD reactor.*

3.2 Fabrication of Porous Si

We anodically etched p-type <100> and <111> Si wafers to form porous Si, and have also etched epitaxially grown Si-C and SiGe layers to form porous structures.

Figure 11 shows the anodic etching system which was used for producing porous Si samples. This system relies on a Keithley Model 225 current source, with the sample connected as the anode (+) and a foil platinum as the cathode (-). The electrolyte, usually a 1:1 mixture of hydrofluoric acid (HF) and ethanol, is contained in a teflon vessel. The silicon wafers were held in a specially prepared jig which only exposes the front surface to the solution, allowing

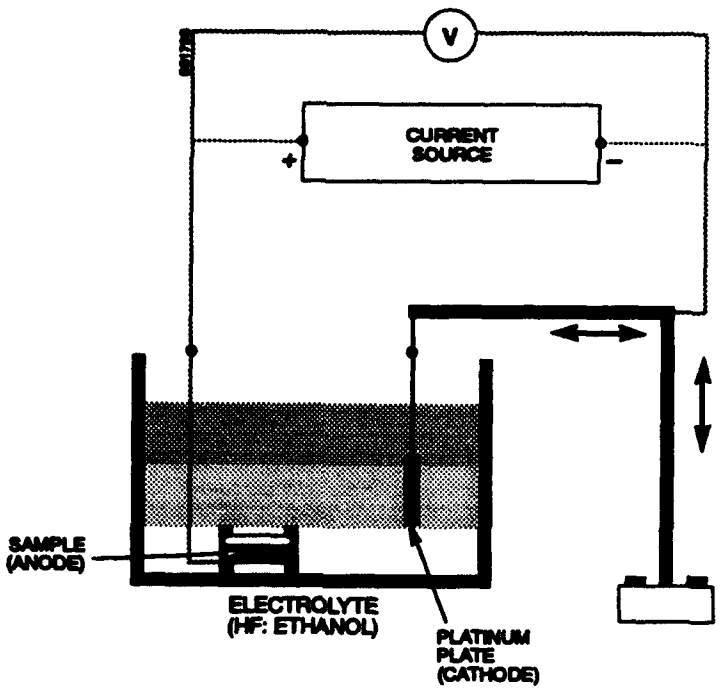

Figure 11 *Schematic diagram of the anodic etching system used at Spire for fabricating porous silicon samples.*

electrical contact from the back, isolated from any liquid. The silicon samples were carefully etched in the HF solution at current densities between 2 and 100 mA/cm^2. We have found that shifts in the emission to shorter wavelengths can be controlled for any sample by increasing the duration of the etch procedure as well as by allowing the samples to remain passively (with no bias applied) in the HF for periods of time after the anodic etching is terminated.

3.3 Carbon Implantation and Annealing

Implantations were accomplished on Spire's high current ion implanter. The beam is generated by an Eaton NV 10-160 joined to a Spire-designed endstation. The beam transport has been modified to produce a variable beam spot area by a mixture of controls using a quadruple triplet lens system coupled to an electronic beam scanning system. The lens creates a focus which can produce a spot as small as 2.5 cm in diameter. This spot is then rastered in a two-dimensional pattern to cover the area of interest. An offset is also introduced to avoid the effects of neutral beam. This system can be used with the raster covering extremely large areas, as great as 40 x 40 cm.

The endstation for this implanter was designed using only semiconductor-compatible materials and geometries. To minimize contamination and maintain flexibility, the main vacuum chamber is very large (27 ft^3) to guarantee that all possible sputtering surfaces are far removed from the wafers. To minimize hydrocarbon contamination, the system uses a 10-inch cryopump and, despite its volume, reaches a base pressure of 1 x 10^{-7} torr. Figure 12a shows the Spire's #5 implanter and Figure 12b shows a system schematic of the implanter.

a)

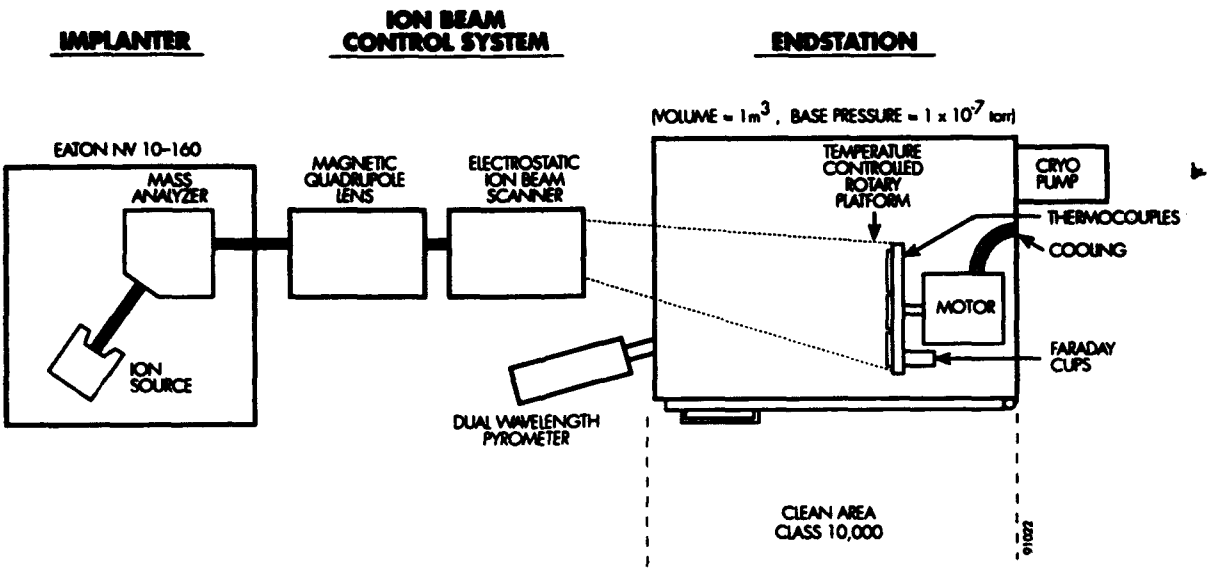

b)

Figure 12 *Spire's ion implanter for high dose implantation and b) schematic of the ion implanter beam transport.*

Following the formation of porous Si layers we implanted carbon into epitaxially grown SiGe layers (Table II), and also porous Si layers and bulk Si substrates (Table III). The substrates were implanted with doses ranging from 1 x 10^{16} to 1 x $10^{17}C^+/cm^2$ at energies from 50 keV to 200 keV. After implantation samples were annealed in an in-house tube furnace to form SiC and SiGeC. Samples were annealed in a nitrogen ambient at temperatures ranging from 500°C to 1300°C for approximately 30 minutes to 3 hours.

Table II *Summary of samples epitaxially grown with GeSi layers of various thicknesses and Ge concentrations.*

	Sample ID	Si Epi	GeSi	%Ge	Si Epi	Carbon Implantation	
						Dose	Energy
SILICON WAFERS	GER1044N	—	500Å	15%	—	1E17	100keV
	GER1023E	—	1000Å	10%	—	1E17	100keV
	GER1022E	—	2μm	10%	—	1E16 2E16	80keV 200keV
	T476	1000Å	2000Å	10%	2000Å	1E16	80keV
	D4662	—	4.72μm	18%	—	5E16	80keV
	GER 1021BE	—	1μm	10%	—	1E17	80keV
	GER1024E	—	300Å	10%	—		
	GER1046B	—	1300Å	11%	—		
	D4709	—	10μm	2.3%	—		

94511

Table III *Summary of carbon-implanted and annealed porous Si, bulk Si and quartz samples.*

Sample ID	Anodization		C-Implantation		Annealing	PL Peak	
	Current (mA)	Etch Time (min.)	Dose 1 x $10^{16}cm^2$	Energy (keV)	Conditions	Wavelength	Relative Intensity
6554-NK3	60	10	10	140	620°C, ½ hrs.	Blue-green light not observed by the naked eye.	
6554-NK4	80	10	10	140	620°C, 3 hrs.		
6554-NK5	100	10	10	140	620°C, 3 hrs.		
AMC-17	25	30	1.4	140	620°C, 3 hrs.		
6554-JF	100	60	1.4	140	620°C, 3 hrs.		
6554-W	75	30	5.5	150	1000°C, 1 hr.		
AMC-2	100	70	5	100	1000°C, 1 hr.		
AMC-3	75	70	1	80	1000°C, 1 hr.		
AMC-8	75	70	5	100	1000°C, 1 hr.		
WA3R	20	15	1	100	500°C, ½ hr.		
AMC-5	100	60	5	100	1000°C, 1 hr.	660 nm	moderate
AMC-17	25	30	1.4	140	1300°C,½ hr.	510 nm	strong
6554-NK3	60	10	10	140	1300°C, ½ hr.	440 nm	moderate
6554-NK4	80	10	10	150	1300°C, ½ hr.	510 nm	strong
6554-NK5	100	10	10	140	1300°C, ½ hr.	-	weak
6554-V	100	60	7.33	50	1300°C, ½ hr.	-	weak
6554-W	75	30	5.5	150	1300°C, ½ hr.	540 nm	moderate
6554-X	100	75	10	50	1300°C, ½ hr.	450 nm	moderate
6554-JF	100	60	1.4	140	1300°C, ½ hr.	450 nm	moderate
AMC-8	75	70	5	100	1300°C, ½ hr.	450 nm	moderate

3.4 Characterization

3.4.1 Optical

Visible Photoluminescence Emission Spectroscopy - PL spectrometry measurements were performed using Spire's PL system, shown in Figure 13. An Omnichrome ultraviolet (325 nm) laser was used to excite porous Si which was implanted with carbon, and for excitation of porous Si produced on epitaxially grown carbon-doped Si films. Porous Si which was fabricated on Si wafers (without epi) was excited mostly with an Argon (488 nm) laser. The laser emissions were dispersed with a SPEX Model 1702/04 grating monochromator and detected with a photomultiplier. An EG&G Model 5207 lock-in amplifier interfaced to a Hewlett-Packard Model 86B computer collected the data.

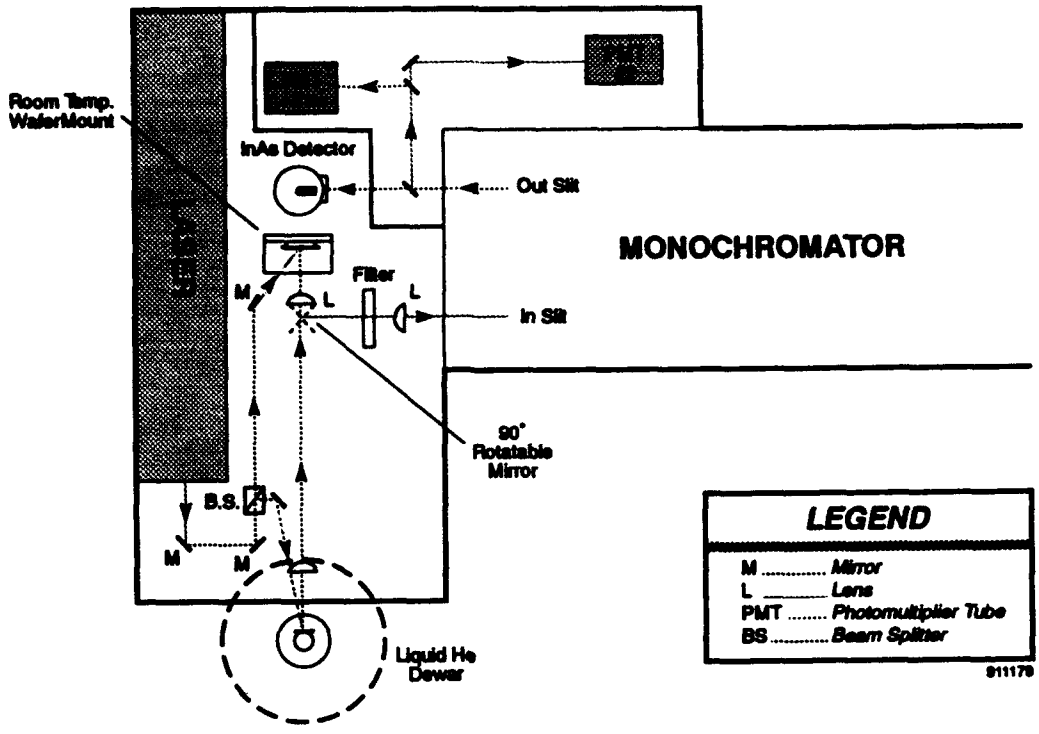

Figure 13 *Schematic of Spire's Pl system.*

Infrared Photoluminescence Emission Spectroscopy - Infrared (IR) PL was carried out at Northeastern University in collaboration with Prof. Clive Perry and Dr. Feng Lu. The IR PL was excited with a Coherent Innova 70 Ar^+ laser, and measurements were carried out for laser powers between 30 to 200 mW. An interference band-pass filter was placed in front of the samples to eliminate plasma lines from the laser beam. The samples were illuminated from the porous Si side and IR PL was collected at a near-backscattering geometry. An SPEX 1401 (0.75m) double monochromator equipped with a pair of 600 line/mm gratings was utilized for the IR PL studies. The PL signal was detected by a liquid nitrogen cooled Northcoast Ge detector. A red filter was placed in front of the detector's collecting lens to filter scattering lines from the second- and third-order grating. Both entrance and exit slits of the monochromator were set at 1000 μm, resulting in a spectral resolution of ~1 nm.

3.4.2 Materials

Rutherford backscattering spectroscopy (RBS) was performed at the University of Connecticut to determine the carbon concentration of the carbon-implanted and epitaxial layers.

Carbon-implanted red-emitting porous Si samples, and porous Si-C epi are being studied by transmission electron microscopy (TEM) in collaboration with Prof. Russell Pinizzatto's group at the University of North Texas and also by Mr. Darold Perry at Purdue University.

Raman spectroscopy and fourier transform infrared spectroscopy (FTIR) spectroscopy measurements were studied by Dr. John Webb at National Renewable Energy Laboratory (NREL).

4 EXPERIMENTAL RESULTS

We assumed that random alloys of SiGe or SiC (with concentrations of a few percent) are required in order to form porous nanostructures of SiC and SiGeC using standard Si processing. This idea was based on work developed at IBM for processing of GeSi. B. Meyerson at IBM has indicated that they have applied standard Si processing to group IV alloys for Si concentrations up to 80%.[23] For that reason we were seeking to grow random Si alloys with concentrations above 80%. We assumed that very extensive work would be required to develop processes to etch SiC (50%/50%) and produce SiC nanostructures with quantum confined properties.

The lattice mismatch of carbon (diamond structure) with Si is about 52% (see Figure 14), therefore, we proposed to grow SiGeC instead of SiC layers on a Si substrate because the presence of Ge atoms could compensate the strain resulting from the Si and C mismatch.

Most models predict an increase in the bandgap of bulk Si with an increase in carbon concentration as shown in Figure 14. Figure 14a shows energy gaps versus lattice parameters for various alloys of silicon, carbon, and germanium; the lattice constants of the Si-C and Si-Ge alloy series, according to Vegard's Law, are shown in Figure 14b. Figure 14c shows the bandgap of SiGe alloys as a function of Ge content for various layers and the bandgap of SiC alloys as a function of C content.

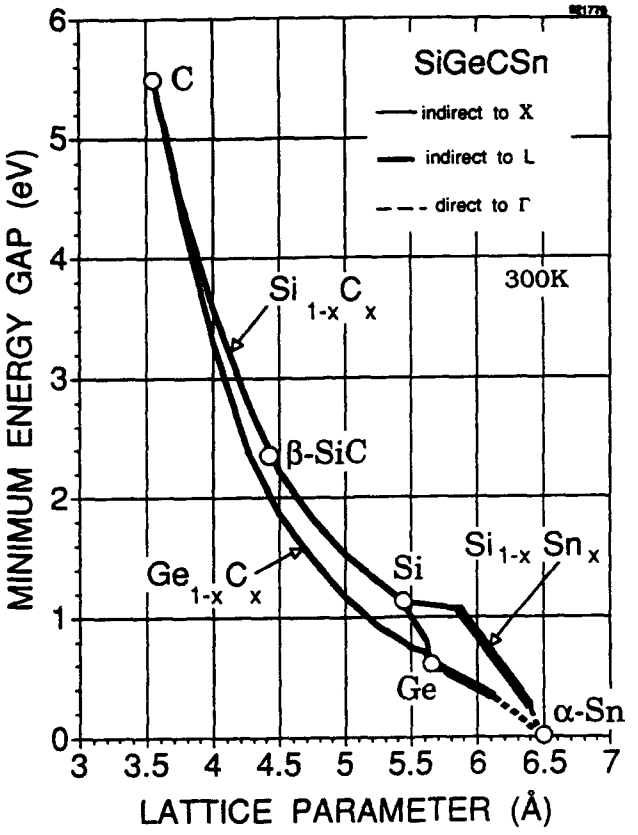

Figure 14a *Estimated optical bandgaps of ordered group IV semiconductor alloys vs. cubic lattice parameter.*[24]

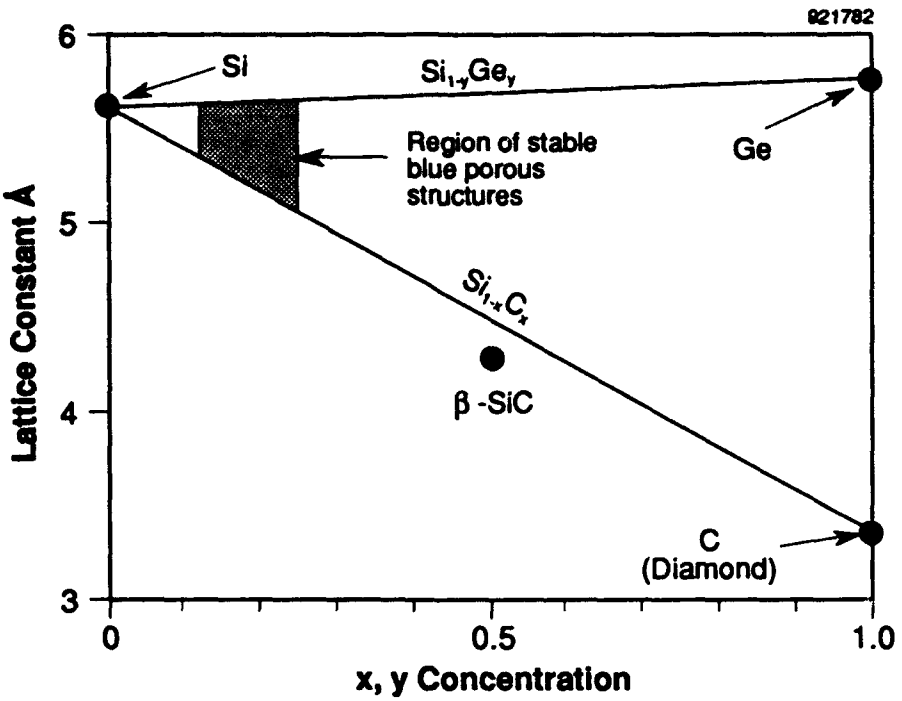

Figure 14b *Cubic lattice parameter vs. composition for Si-C and Si-Ge alloys, based on Vegard's Law.*[24]

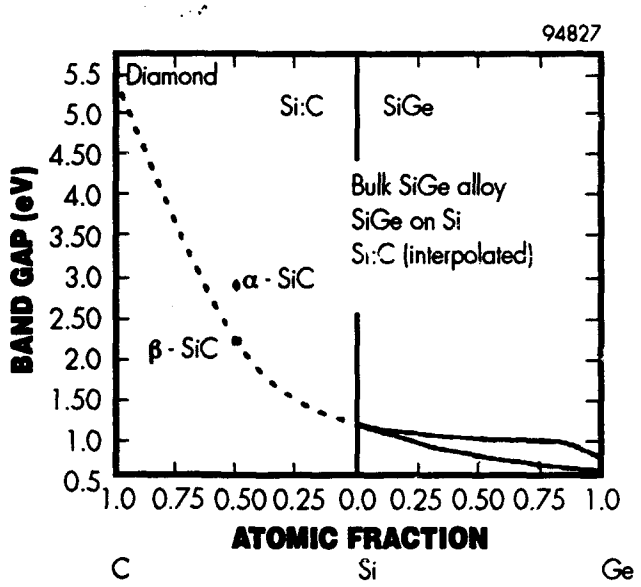

Figure 14c *Measured bandgap of $Si_{1-x}Ge_x$ alloys as a function of Ge content for bulk (upper curve) alloys and layers pseudomorphic to Si (lower curve), and the estimated bandgap of $Si_{1-y}C_y$ alloys as a function of C content. The estimate is based on a spline fit through the gaps for Si, β-SiC and diamond. Also shown is the gap for α-SiC. The top scale shows the strain in the film for growth on Si.*[25]

Silicon, carbon, and germanium all crystallize with the cubic diamond structure. By forming alloys between silicon and carbon, a metastable phase with a bandgap of greater than 1.1 eV can be achieved, and blue-emitting porous structures will be demonstrated.

In the course of Phase I work, we came to the idea that instead of modifying the bandgap of bulk Si-based materials, it would be easier to change/enlarge the bandgap of Si nanostructures. A simple way to test this concept, was to implant carbon into Si nanostructures in order to form Si-C or SiC quantum confined nanostructures. This idea was strengthened by an AF SBIR program in which we demonstrated for the first time strong room-temperature infrared (1.54 μm) PL from erbium-implanted porous Si.

Epitaxial Growth of SiGe Layers - The growth of a SiGeC phase has been limited by both the complexity and difficulty of the process and the time and funding limitations of the program. This motivated us to seek a new and easier method to form Si-based blue-green light-emitting materials. We started with SiGe epitaxial layers which were grown by high atmospheric-temperature CVD. Table II shows samples with SiGe layer thicknesses ranging from 500Å to 10 μm. Typical RBS results of a thin (<2000Å) and a thick (few microns) SiGe layer are shown in Figure 15.

SiGe samples were anodically etched and PL was measured with an argon laser at 488 nm and 90 mW of power. SiGe porous structures were implanted with a dose in the range of 1×10^{16} to 1×10^{17} C^+/cm^2 at energies of about 80 keV to 200 keV, and annealed from 500°C to 1050°C for 15-60 minutes. Figure 16 shows typical PL results obtained from an anodically etched SiGe sample with a thickness of 1 μm and a Ge concentration of 10% after annealing at 1050°C for 15 minutes in N_2. Figure 16 also shows a PL spectrum from the same sample after implantation with a dose of 1×10^{17} C^+/cm^2 and annealing; the carbon implantation was performed using a mask with circular dimensions of approximately 5 mm. These spectra were obtained right after the samples were annealed. An interesting feature of this spectra is that the carbon implanted and annealed sample is relatively stronger than porous SiGe (for measurements performed directly after annealing) and the peaks of both samples did not shift. Note that after aging the samples for three months in the lab, we studied the samples again by PL (see Figure 17). No shift in peak position occurred, however, the intensity of porous SiGe increased over time while the intensity of porous SiGeC decreased over time. We believe this comparison is reliable since we used PL from standard $Al_{.30}Ga_{.70}As$ as a reference for both groups of measurements to calibrate the PL facility.

Epitaxial Growth of SiC Layers - We have grown several groups of SiC random alloy films, with thicknesses of 8 to 10 μm, on <111> Si substrates. Groups of samples were differentiated by the amount of methane gas flow (source for carbon) during epi growth. The Si substrates used were both 2-inch and 4-inch wafers; details are listed in Table IV. We used different techniques such as high resolution X-ray diffraction (HR-XRD) and FTIR to obtain information about these materials. Figure 18 shows typical results of HR-XRD indicating a SiC peak is present. Lattice contraction caused by carbon doping of Si <111> has been determined by rocking curve measurements using Cu $k_{\alpha 1}$ radiation and (333) reflections. The perpendicular lattice constant mismatch between the substrate and the Si-C layer varies linearly with the carbon doping level. Following the procedure described by Hoke *et al.*[26] we have determined that the carbon concentration (N_c) of the sample in Figure 18 is about 1.07×10^{19} cm^{-3}, which corresponds to 0.02%.

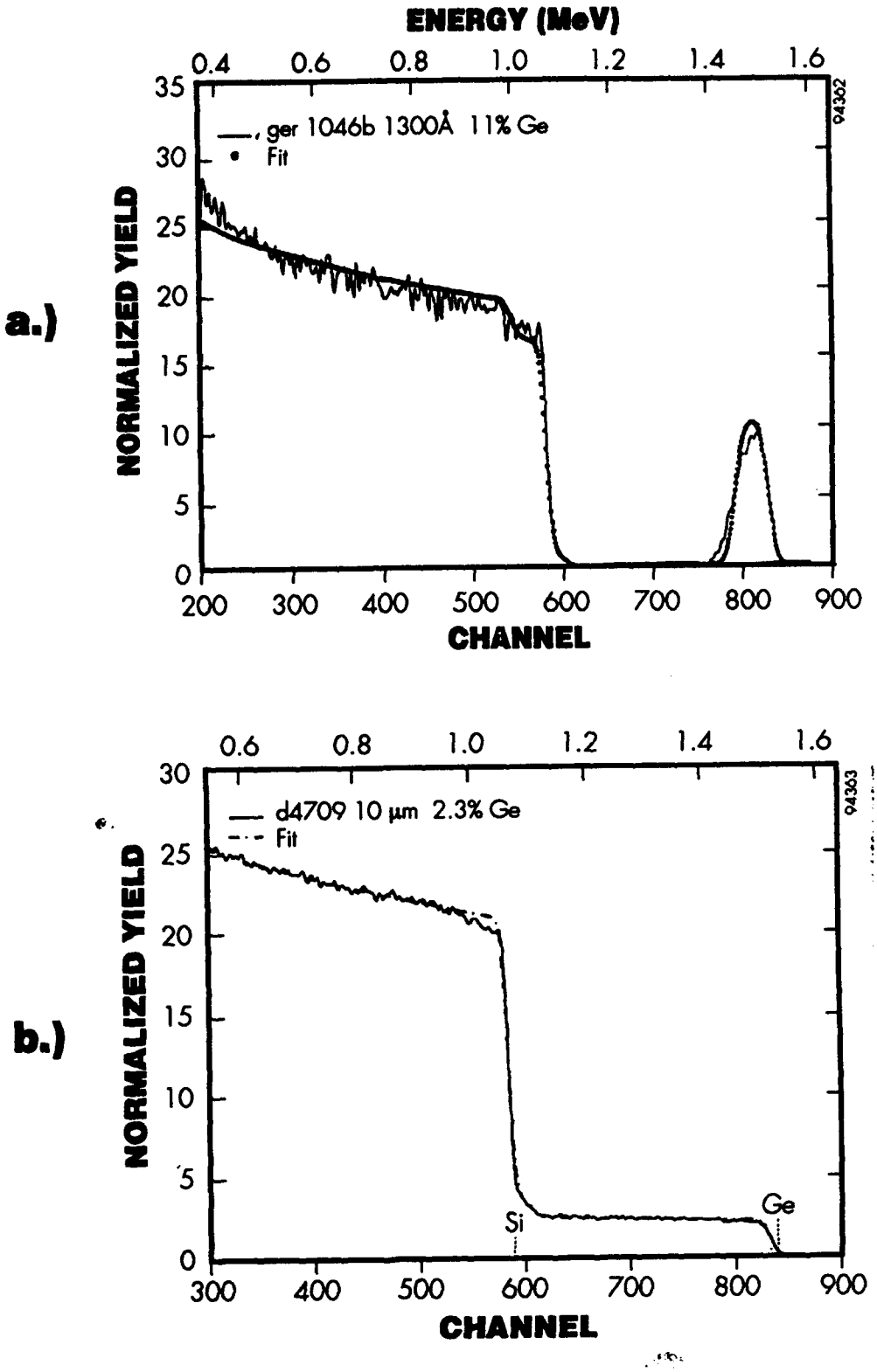

Figure 15 *RBS (using the RUMP code) of epitaxially grown SiGe layers a) a thin layer approximately 1300Å thick, and b) a thick layer about 10 µm thick.*

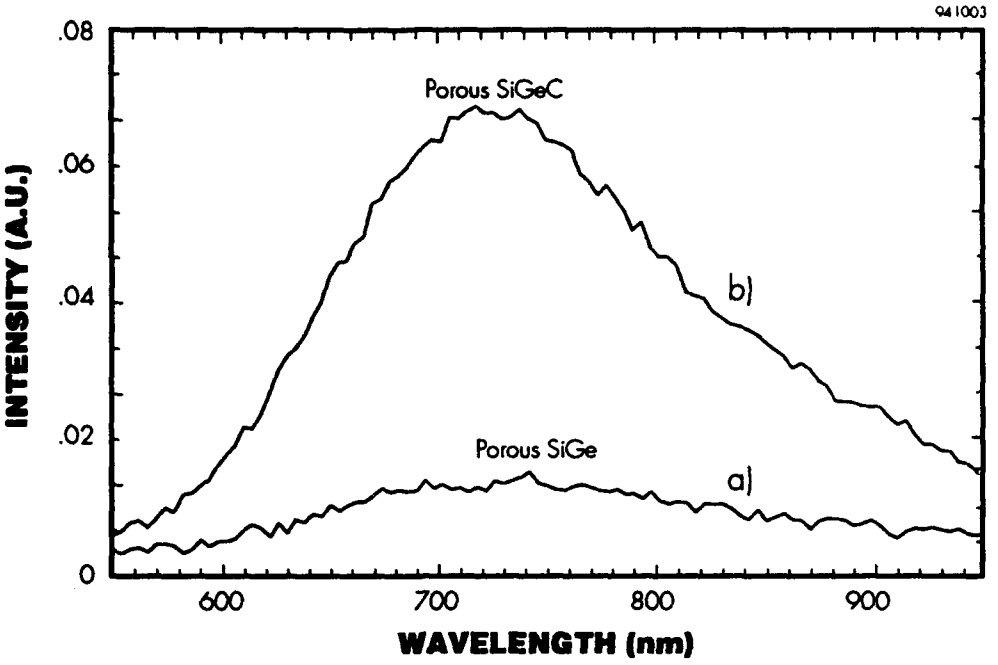

Figure 16 *PL spectra from a sample epitaxially grown with 1 μm of SiGe a) anodically etched to form porous SiGe, and b) anodically etched and implanted with carbon to form porous SiGeC. Both measurements were performed right after annealing.*

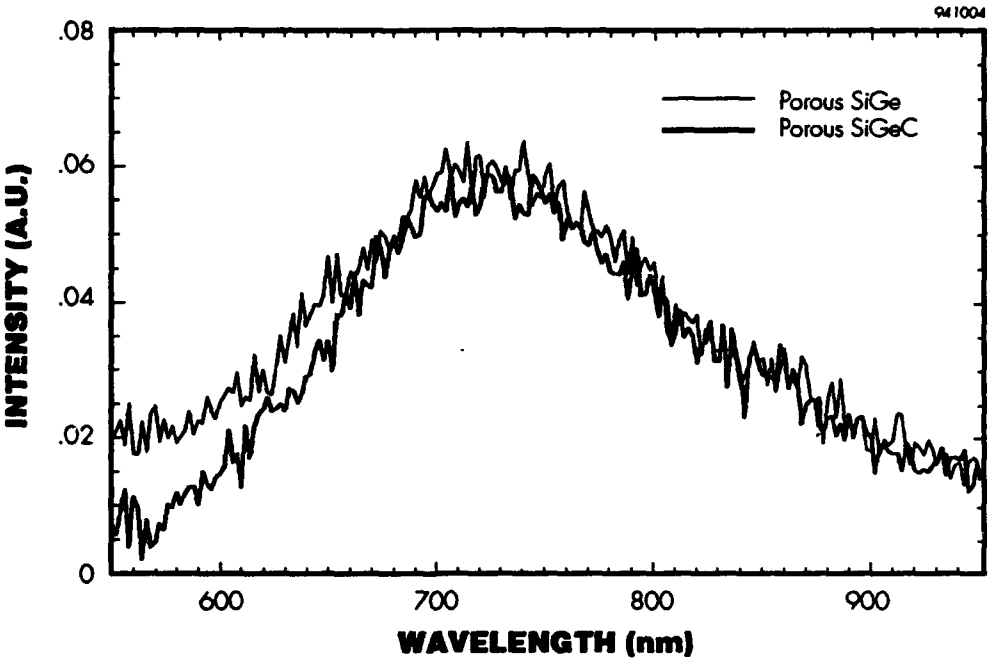

Figure 17 *PL spectra from the sample whose PL is shown in Figure 16, after the sample had aged for three months in a lab environment. No shift in peak position was observed, however, the intensity of the porous SiGe increased and the intensity of the porous SiGeC decreased over time.*

Table IV *Summary of samples with Si-C layers epitaxially grown with various concentrations of methane gas flow.*

2" Substrates - B<111> .15 - .25Ωcm					
Sample #		**Dopant s.p. (C)**	**Bake Temp**	**Nom. Thickness**	**Dopant**
F2017	CA CB	30% of max. methane flow rate	1053°C	8μm	Methane
4" Substrates - B<111> .002 - .005Ωcm					
Sample #		**Dopant s.p. (C)**	**Bake Temp**	**Nom. Thickness**	**Dopant**
F2018	CA CB	50% of max. methane flow rate	1120°C	10μm	Methane
F2019	CB CC	70% of max. methane flow rate	1120°C	10μm	Methane
F2020	CC CE	85% of max. methane flow rate	1120°C	10μm	Methane
F2021	CA CC	100% of max. methane flow rate	1120°C	10μm	Methane

94512

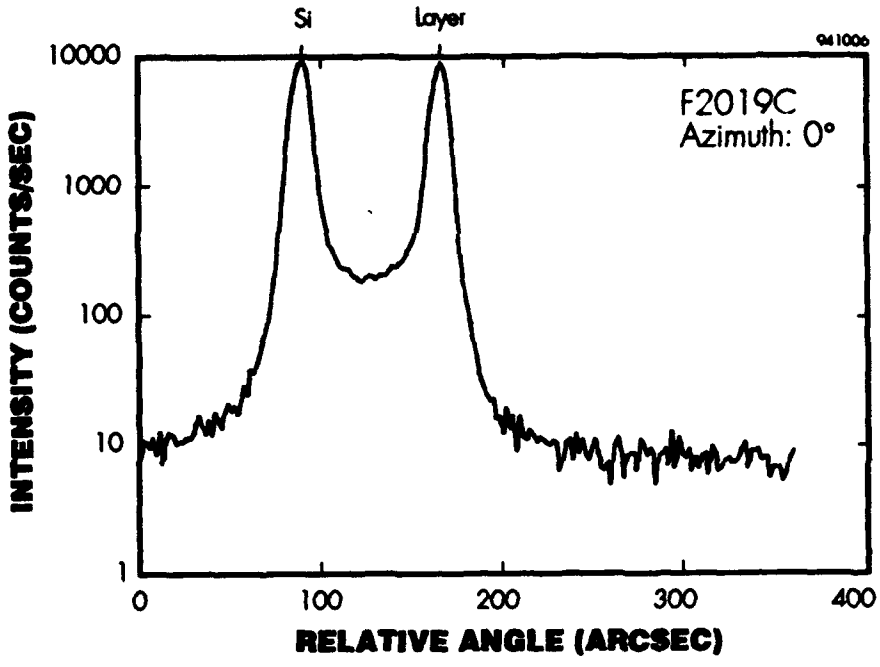

a.)

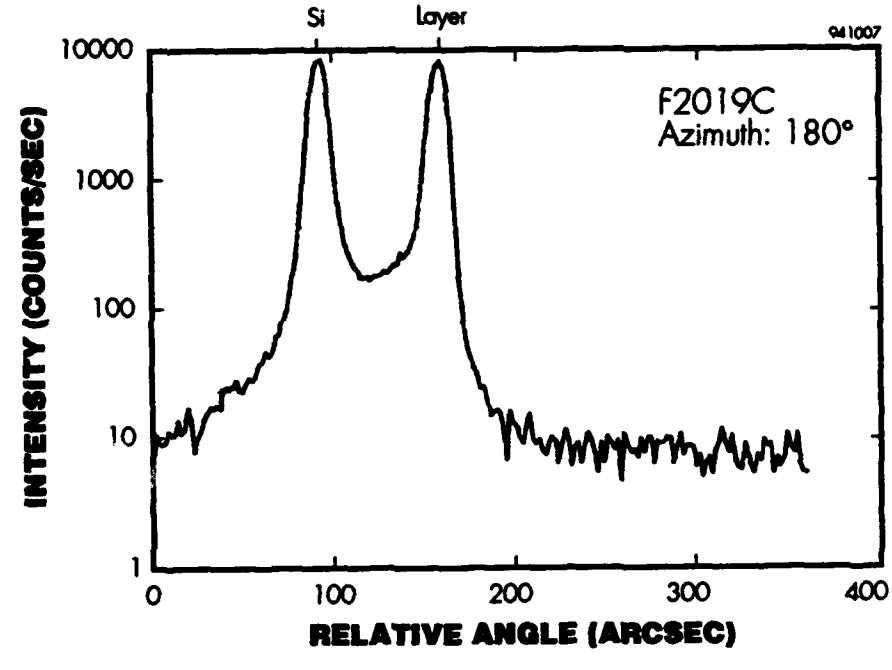

b.)

Figure 18 *High resolution X-ray diffraction of an epitaxially grown Si-C layer on a Si substrate measured a) with wafer at O° and b) wafer after rotation at 180°. Using the procedure by Hoke et al. we determined the carbon concentration was about 0.02%.*[26]

Further information about the position of carbon atoms in Si has been obtained by FTIR spectroscopy. Figure 19 shows FTIR of an epitaxially grown carbon layer on a Si <111> substrate with a maximum gas flow of 30% (sample F2017A). A strong absorption line at about 600 wavenumber has been observed which corresponds to substitutional carbon, proving that Si-C random alloys are formed. It should be noted that absorption at about 600 wavenumber is from the Si-C epi layers since none of the Si substrates showed a similar absorption line. In Phase II we may determine the precise amount of carbon using secondary ion mass spectrometry (SIMS).

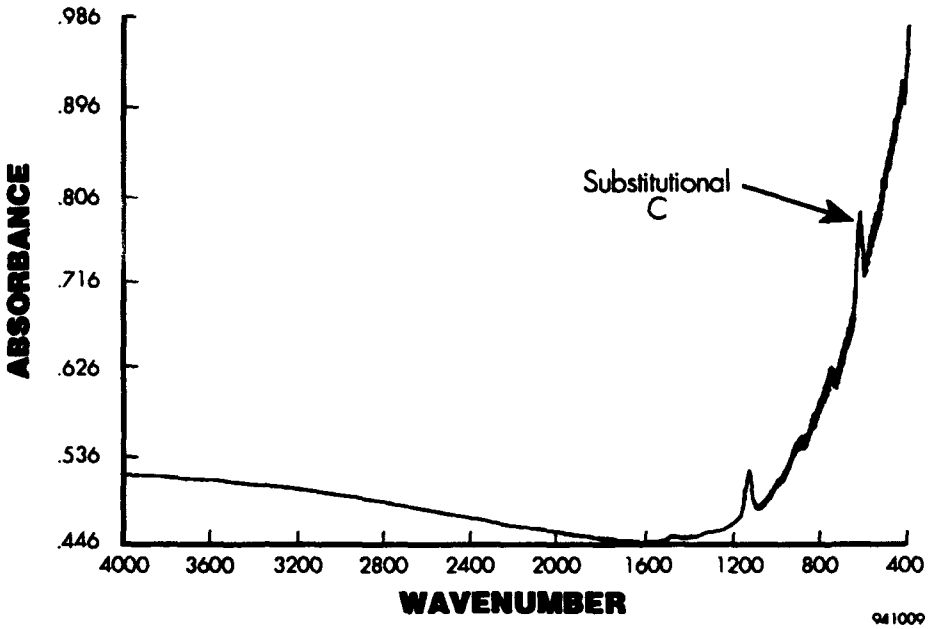

Figure 19 *FTIR spectra of a carbon-doped Si epi layer showing a strong absorption line at 600 wavenumber which corresponds to substitutional carbon, see Figure 24.*

We have etched some of the Si-C wafers by our standard anodic etching methods and have observed very strong red-emitting photoluminescence, this red PL was stronger than any we have previously observed. We speculate that such a strong red emission may be from a rather impurity (metals) free Si epilayer. Note that bulk Si produced by standard processes contains trace elements with a large number of impurities including transition metals. Figure 20 shows a PL spectrum from the porous Si-C sample and Figure 21 and 22 are photographs of the same red-emitting porous sample showing that its emission is as strong as, or stronger than, that of a standard color PC monitor. Our bulk Si-C and porous Si-carbon structures were studied by RBS, however, RBS is not sensitive to concentrations of carbon below 10%. Since we did not observe any carbon effect in our samples, we believe the concentrations were below 10%.

Comparison of the PL from porous epitaxial Si-C with that from a standard $Al_{.30}Ga_{.70}As$ sample indicated that the intensity of our porous epitaxial Si-C is about seventy times greater than that from the $Al_{.30}Ga_{.70}As$. Because the intensity of PL emission is dependent on doping level and etching conditions, a direct comparison of intensity and peak position of these samples, with those from standard silicon samples, is impossible. Only a qualitative comparison can be made. During the past few years, we have etched several hundred Si wafers with different doping levels and under different conditions. This red PL appears stronger to us than any previously observed samples prepared under any etching conditions.

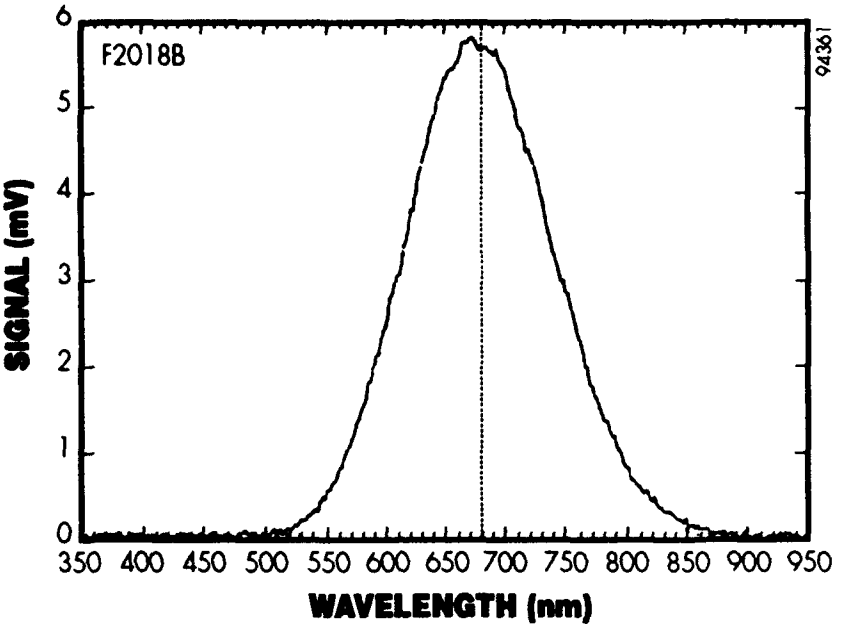

Figure 20 *PL spectrum from a Si-C porous structure fabricated from anodically-etched epitaxial Si-C.*

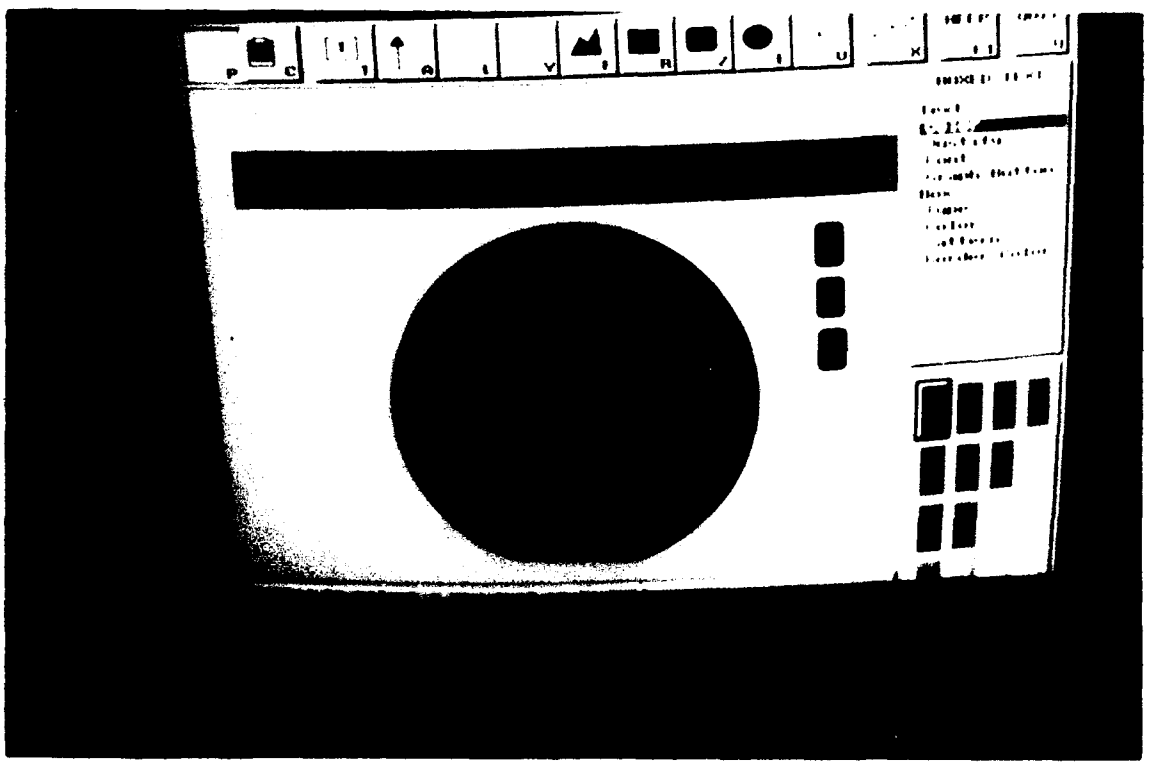

Figure 21 *Photograph showing a red-emitting porous Si-C sample, fabricated from an anodically-etched CVD grown Si-C layer, which was mounted on a color PC monitor in the dark to compare the uniform color and intensity of the sample.*

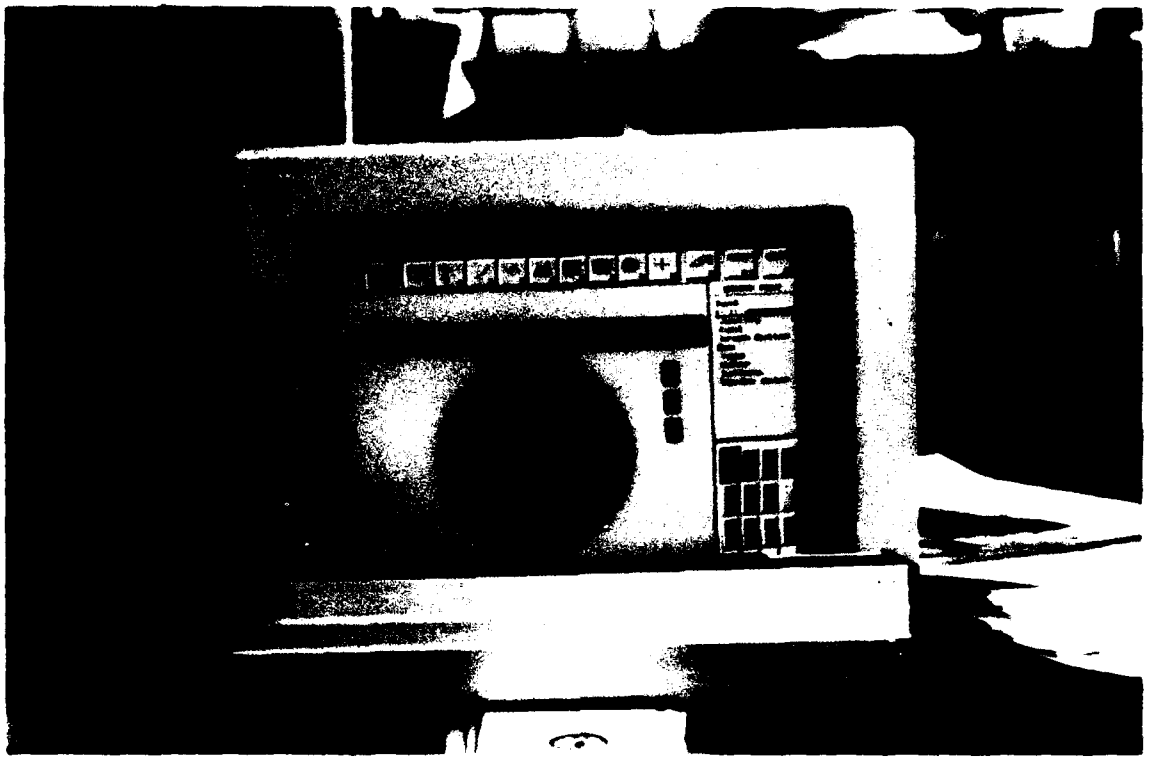

Figure 22 *Photograph showing a red-emitting porous Si-C sample, fabricated from an anodically-etched CVD grown Si-C layer, which was mounted on a color PC monitor in room light to compare the uniform color and intensity of the sample.*

Based on present results, one could argue that the strong red emission may be due to an impurity-free Si epi layer, whereas bulk Si contains trace elements of a large number of impurities, including transition metals, which could reduce the PL intensity. Although we do not have absolute proof, we speculate that the strong emission is due to the bandgap change because of the presence of carbon.

From the porous Si spectrum in Figure 20 we cannot conclude whether a blue shift occurred due to the growth of epitaxial Si-C. On the other hand, as we will show in the next section the introduction of a high concentrations of carbon into porous Si could enable the fabrication of blue-green light-emitting devices.

4.1 Blue-green Emission From Carbon-implanted Porous Si

One method to obtain blue-green emission from porous structures is to transform Si nanostructures which emit red light into Si carbide nanostructures which may emit blue-green light. This basic method involves using carbon implantation and annealing to form a SiC phase. We have developed a recipe to form a SiC phase in bulk Si using the implantation method. Depending on implantation and annealing conditions, one may obtain poly- or single-crystal SiC structures.

Figure 23 shows a typical plan-view TEM and an electron diffraction pattern of a sample implanted below 400°C at 80 keV into a Si substrate followed by annealing at 1300°C. The electron diffraction pattern of the real surface region is shown in Figure 23b. The rings corresponding to SiC <111> with a d-spacing of 2.52Å, and <200> reflections with a d-spacing of 2.18Å are observed in this micrograph which indicate the formation of β-SiC.

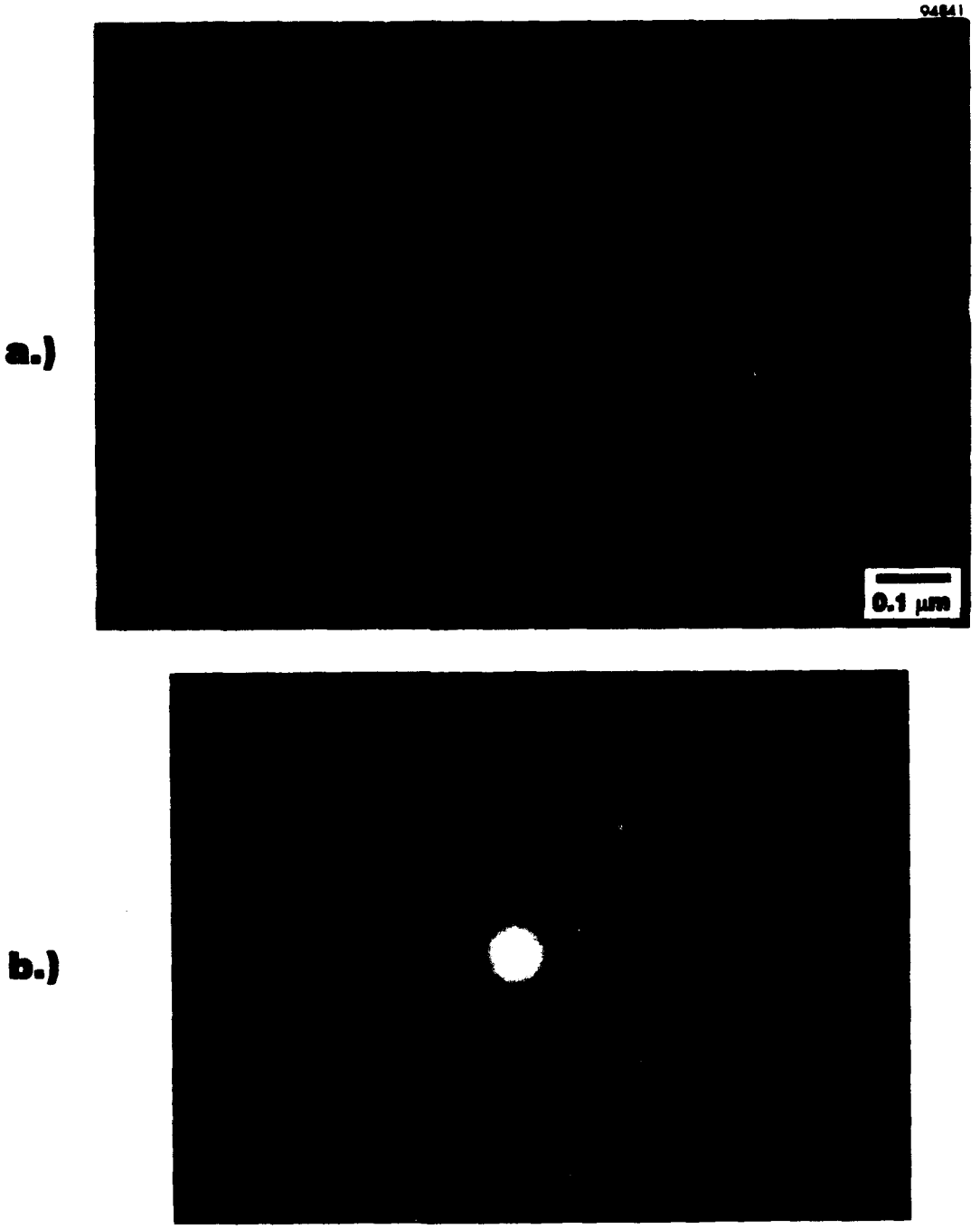

Figure 23 *Bulk Si implanted with carbon and annealed at 1300C; a) plan-view TEM image of the near surface region showing polycrystalline SiC, and b) the electron diffraction pattern of the near surface. Two rings corresponding to reflection from SiC <111> and <200> planes are shown.*

We have also applied FTIR to study SiC. C-implanted and annealed Si substrates were used in this study as a reference for comparison with C-implanted Si nanostructures. Figure 24 shows FTIR data for C-implanted with a dose of 1.2 x 10^{18} C/cm^2 and annealed at high temperatures shows clearly an absorption line above 800 cm^{-1} which is generally observed from SiC material[27] and the line from about 600 cm^{-1} is typically observed from substitutional carbon in Si.[28]

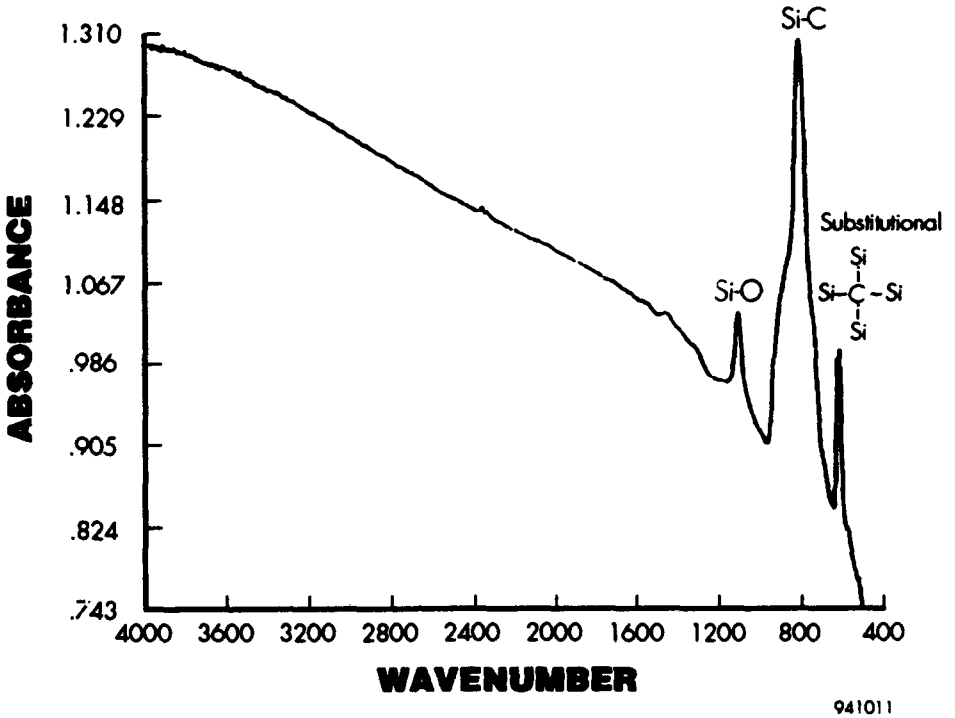

Figure 24 *FTIR spectrum from a thin film SiC layer formed by carbon implantation and annealing of a Si substrate indicating an absorption line at about 829 cm^{-1}.*

We anticipated that since SiC forms in a bulk Si substrate we should be able to produce SiC nanostructures by implanting carbon into Si nanostructures with quantum confined properties. Carbon was implanted into several three-inch p-type porous Si substrates at energies of 50 to 150 keV with doses ranging from 1 x 10^{16} to 1 x 10^{17} C$^+$/cm^2 using an in-house ion implanter with rastered beam scanning. A comparison of PL spectra from a porous Si sample before and after carbon implantation shows that carbon implantation resulted in a reduction in PL intensity.

C-implanted samples were annealed in N_2 at temperatures ranging from 500 to 1000°C for about 15 to 60 minutes, however, no blue-green light emission was observed. On the other hand, once samples were annealed at 1300°C a strong blue-green PL could be observed with the naked eye. Figure 25 shows PL results of a porous Si sample before implantation, after implantation (with a dose of 1 x 10^{16} C/cm^2 at 100 keV), and after implantation and annealing at 1300°C. Both the unimplanted and C-implanted unannealed samples were excited at 488 nm at 100 mW. The annealed sample was excited with a UV laser at 325 nm at 9 mW of power. The intensity of these samples was normalized to the same height for comparison. From several samples we studied, the sample in Figure 25 had the strongest blue emission. Figures 26 and 27 show PL results of porous Si samples before implantation and after implantation and annealing at 1300°C; and Figure 28 shows PL results of a carbon implanted porous Si sample before and after annealing.

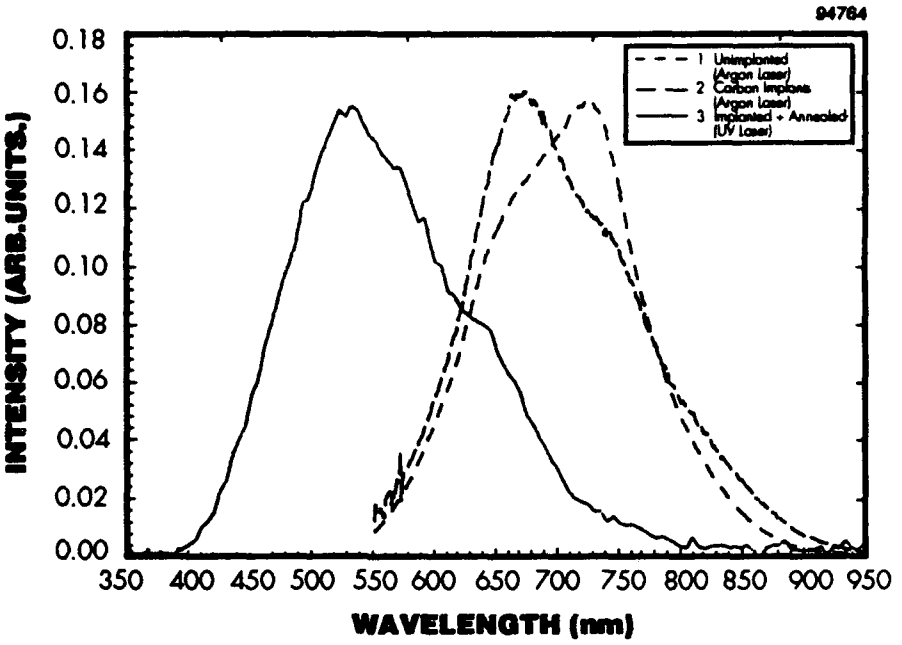

Figure 25 *Normalized spectra of visible PL from a porous Si sample before implantation, after implantation, and after implantation and annealing at 1300°C. These spectra indicate a transformation from a red-emitting porous structure to a blue-green emitting structure.*

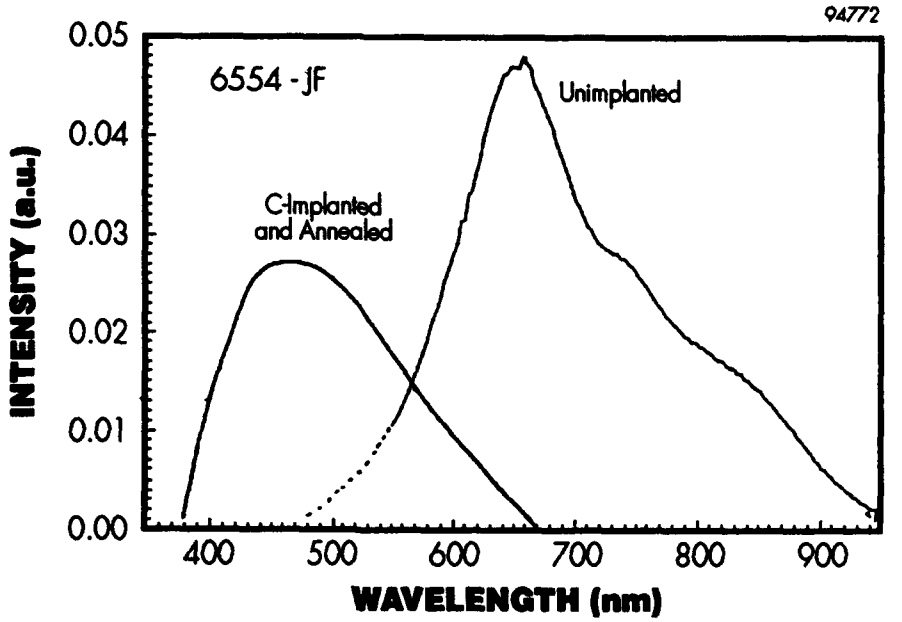

Figure 26 *PL spectra from a porous Si sample (6554-JF) before implantation and after implantation with a dose of 1·4 x $10^{16}C^{+}/cm^{2}$ and annealing.*

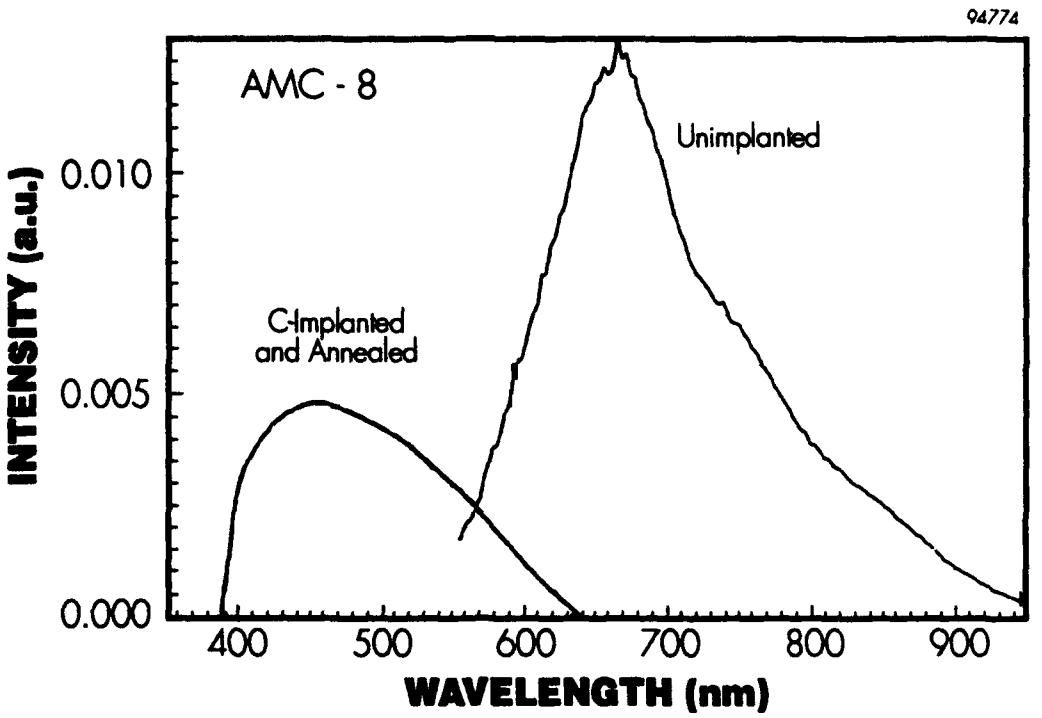

Figure 27 *PL spectra from a porous Si sample (AMC-8), before implantation and after implantation with a dose of 5 x $10^{16}C^{+}/cm^{2}$ and annealing.*

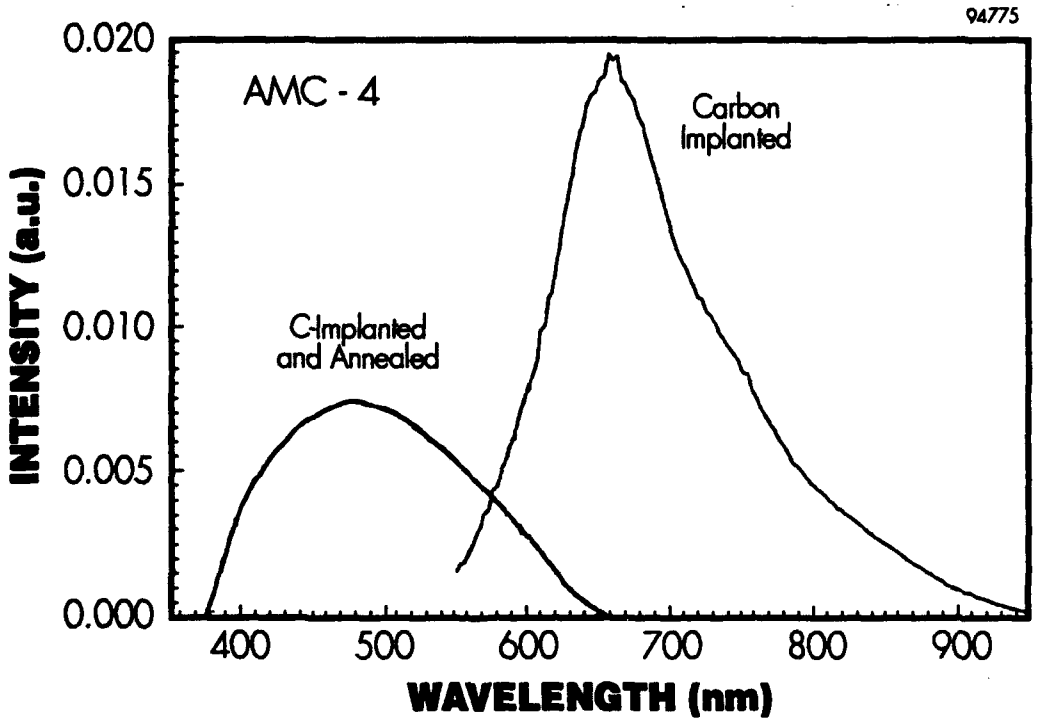

Figure 28 *PL spectra from a porous Si sample (AMC-4), implanted with a dose of 5 x $10^{16}C^{+}/cm^{2}$, before and after annealing.*

Figures 26 to 28 show a shift to blue wavelengths after carbon implantation and annealing at high temperatures. The C-implanted and unimplanted samples were excited at 488 nm at 100 mW. The implanted and annealed samples were excited with a UV laser at 325 nm at 9 mW of power. Comparing spectra from a carbon-implanted and annealed sample with an $Al_{.30}Ga_{.70}As$ reference sample indicates that green-blue emission from the carbon-implanted porous Si was 20 times stronger than the $Al_{.30}Ga_{.70}As$ sample. A comparison of the intensity from an unimplanted porous Si sample with an $Al_{.30}Ga_{.70}As$ sample shows that the intensity of the red emission is a factor of 4 stronger than the $Al_{.30}Ga_{.70}As$.

As mentioned above we have implanted several samples with carbon using a variety of doses. Some of the C-implanted and annealed samples did not emit blue light therefore it appears that emission is dependent on the sample history e.g. etching and implantation conditions.

As this report was prepared a paper was published by T. Matsumato *et al.*, which reports blue-green luminescence from anodically-etched SiC (see Figure 29). To fabricate their porous SiC they have used 6H-SiC type single crystal with an indirect bandgap of 2.86 eV (our SiC material has a bandgap of 2.2 eV).[29] Our porous SiC results are very comparable. Nonetheless, our work has a significant advantage because it can be integrated into advanced Si-based technology. Using our technique, the porous Si material (compatible with Si circuitry) can be selectively implanted with carbon to achieve blue emission. Annealing of our material is very important and could eventually be performed by simple laser annealing.

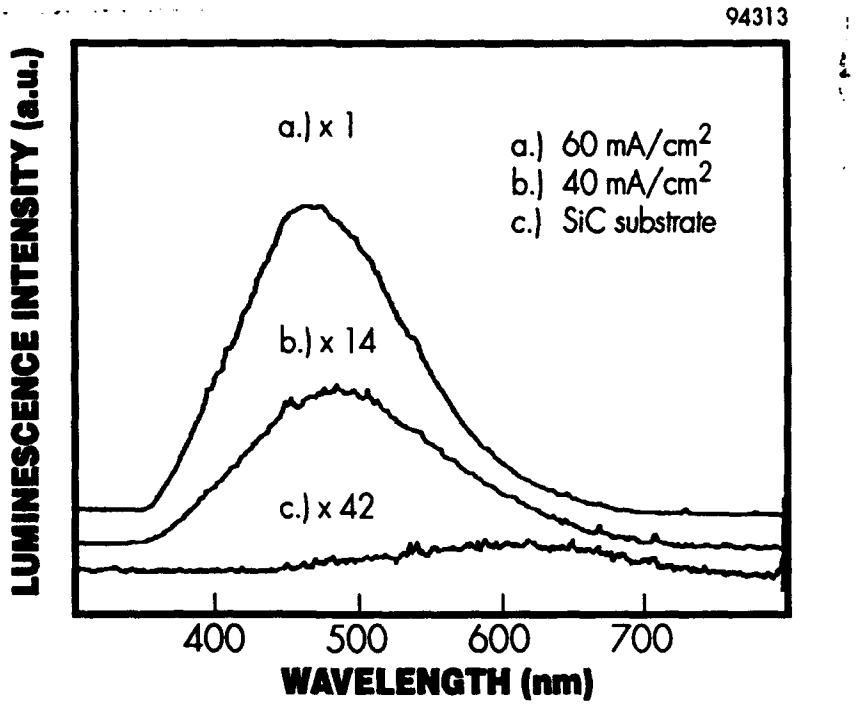

Figure 29 *Luminescence spectra from porous SiC for an anodization current density of a) 60 mA/cm², b) 40 mA/cm², and c) results for crystalline 6H-SiC.*[18]

4.2 Origin of Blue-green Emission from C-implanted Porous Si

It is very important to understand the origin of blue-green emission from carbon-implanted red-emitting porous Si. We anticipated that, by converting nanocrystallites of red-emitting Si into SiC nanocrystals, blue-green emission could be obtained due to the quantum confinement effect. To establish this point, we must determine whether or not SiC nanoparticles are formed in the porous structure. Therefore, we have been very interested in directly observing SiC nanostructures in the porous layer, and have sent blue-green emitting samples for XTEM measurement. Specimen preparation for XTEM measurements of porous SiC nanoparticles in porous Si is very complicated because a) it has never been done before and b) the ion beam milling rate of Si is much higher than for SiC particles; therefore, very often the specimen is destroyed.

Electron diffraction measurements were performed at AMER-TEM, on a blue-green emitting porous Si sample as shown by Figure 30. Reflections at <111> and <200> planes were clearly observed which prove that a β-SiC phase is present in the porous structure. In previous work we have demonstrated the presence of Si nanosparticles, and are interested in observing actual SiC nanostructures from these samples. However, the facilities at AMER-TEM did not provide high enough magnification power to observe actual SiC nanostructures, hence, we are waiting to receive further data from Purdue University and the University of North Texas.

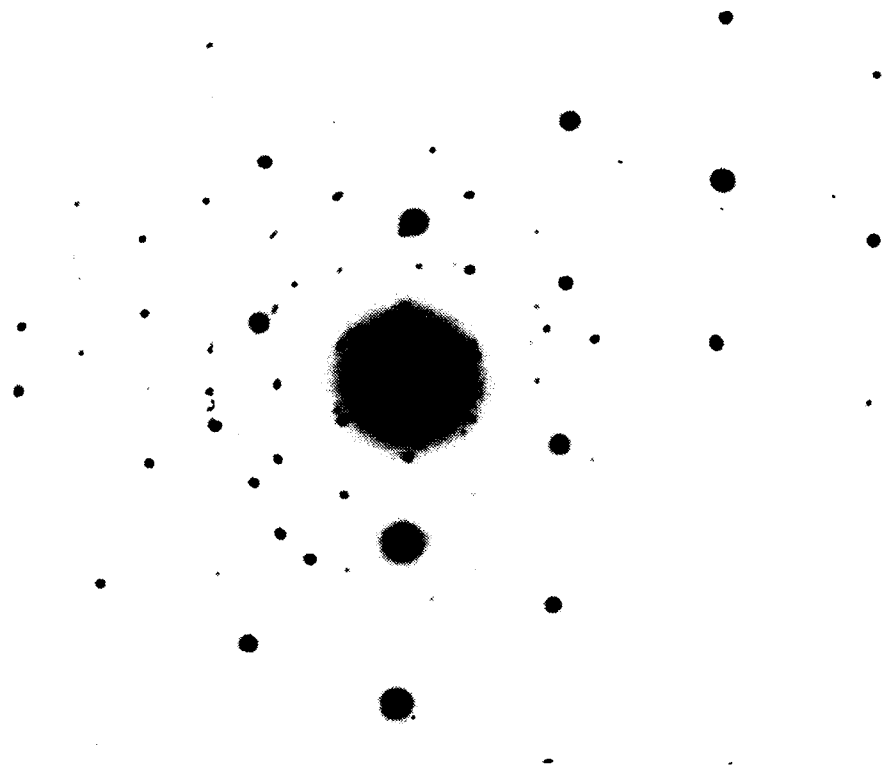

Figure 30 *Spots corresponding to <111> and <200> reflections of SiC are present in the electron diffraction pattern of a blue-green emitting porous Si sample, thus providing proof of a SiC phase.*

Recently we have received preliminary catholuminescence (CL) data from Professor Pankove's group at the University of Colorado at Boulder. Figure 31 shows CL data from a carbon-implanted porous Si sample measured at room-temperature and 5.7K. As shown there is a light emission at about 1.80 eV and 2.80 eV which corresponds to blue and orange light emission. This CL data is in agreement with our PL results measured at Spire.

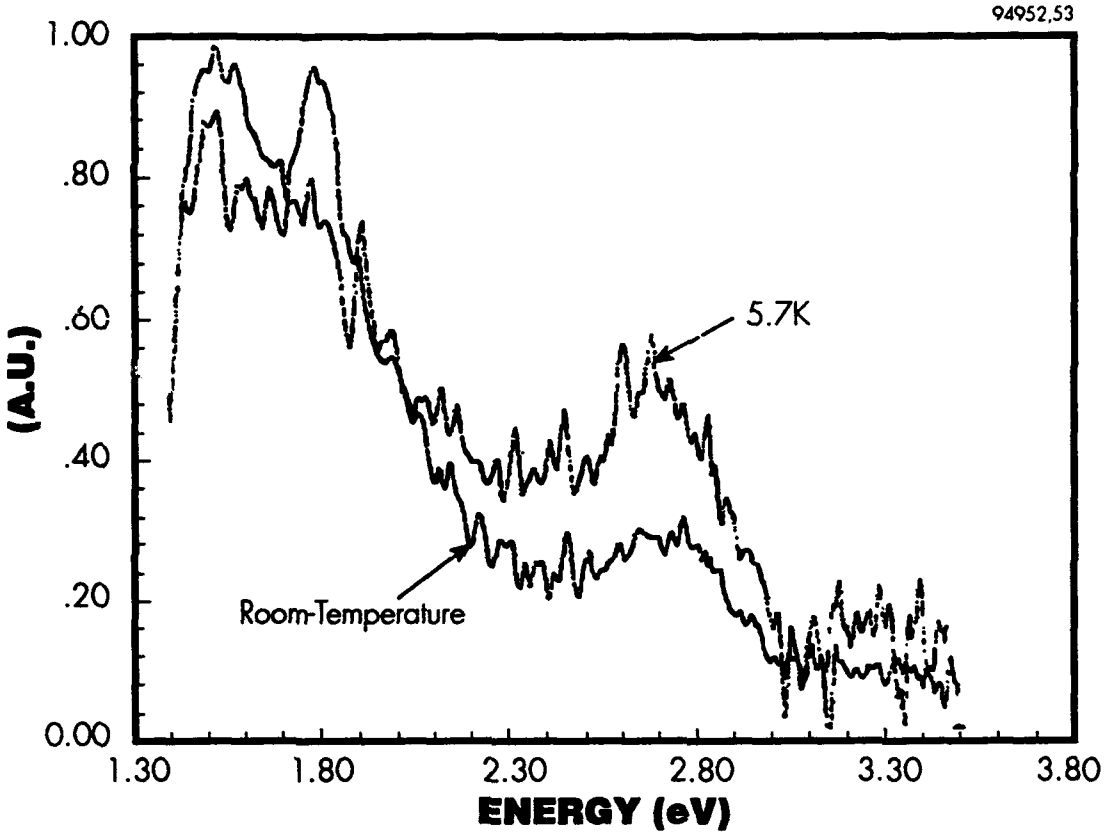

Figure 31 *Preliminary CL data from the University of Colorado by Professor Pankove's group indicating blue and orange emission from C-implanted and annealed porous Si.*

The presence of SiC has also been confirmed by FTIR measurements performed in collaboration with scientists at NREL. Figure 32 shows FTIR spectra of red-emitting porous Si before C-implantation, after C-implantation but unannealed, and after C-implantation and annealing at 1300°C. Figure 32c shows a strong absorption line at about 800 cm^{-1} which is typically observed from SiC.[27] This absorption line coincides exactly with FTIR from carbon-implanted bulk Si (Figure 24). Note that Figure 23 has again verified the formation of β-SiC. Based on the above data we may deduce that green-blue emission is from SiC with quantum confined properties.

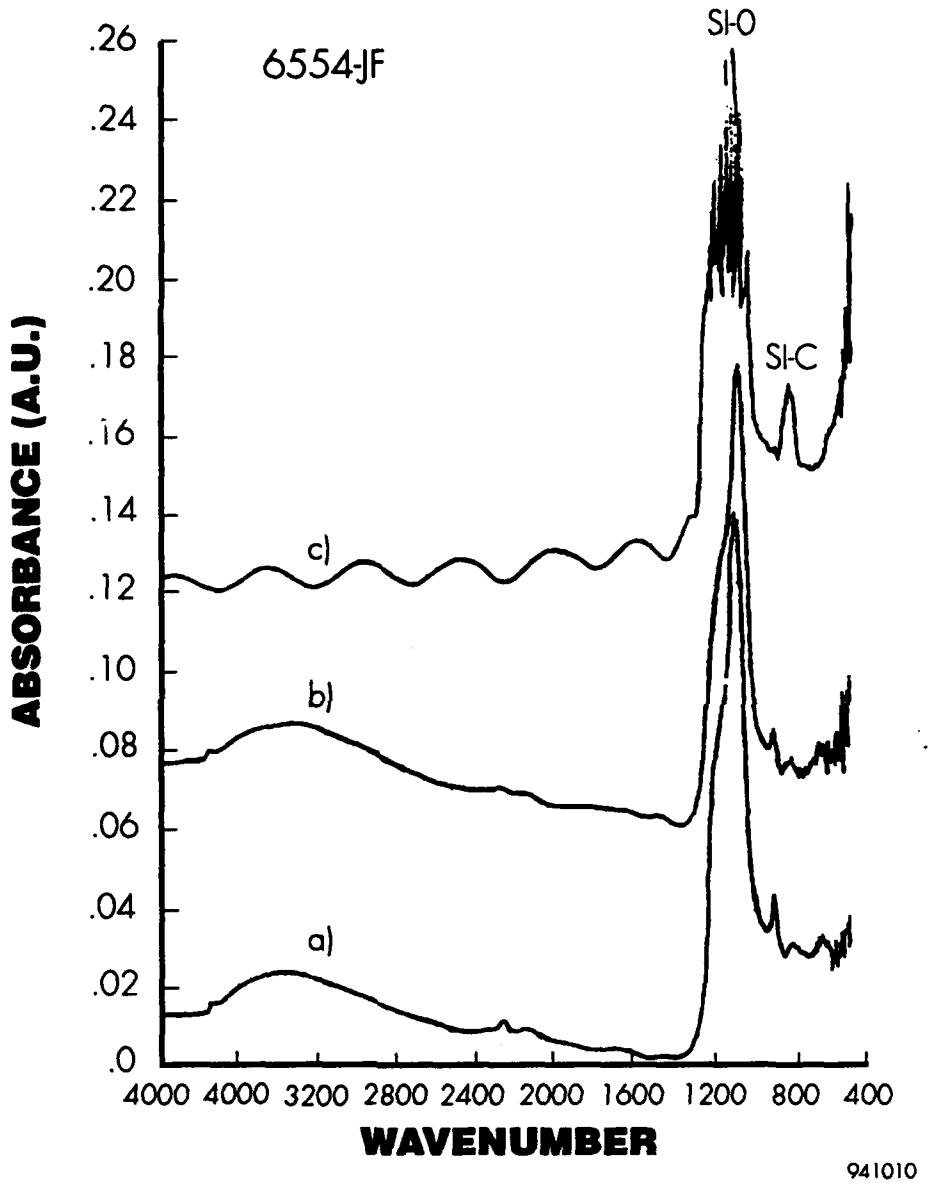

Figure 32 *FTIR spectra of a) red-emitting porous Si and b) C-implanted and unannealed porous Si, and c) C-implanted and annealed blue-green-emitting porous Si with an absorption line which is identical to that reported for SiC.*

4.3 Infrared Emission from C-implanted Samples

In addition to blue-green emission from the C-implanted and annealed samples we also observed very strong infrared emission at room-temperature. Figure 33 shows infrared PL spectra measured from room temperature to 10K which demonstrates the presence of peaks from 1000 nm to 1400 nm. Since the interest of this work was visible light emission, we did not elaborate on these results in this report. However, the peak at 1400 nm could be useful for optical communications in fiber optics. In Phase II we may address the application of infrared emission if it is determined by the government to be useful.

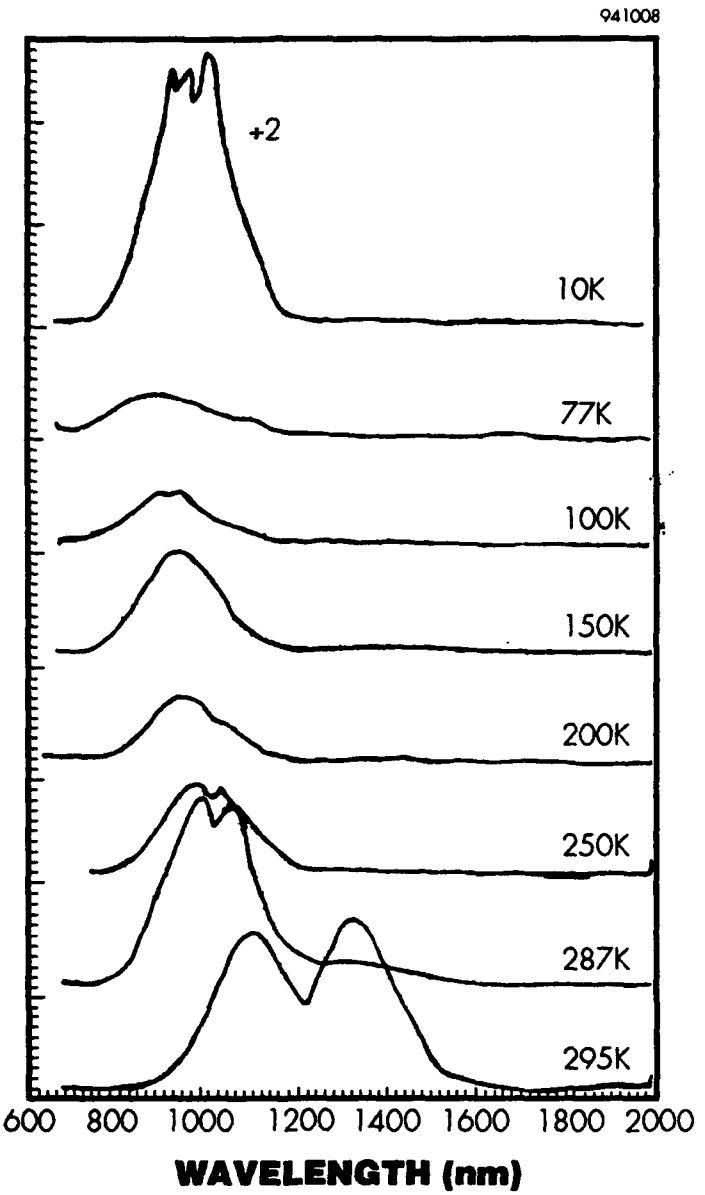

Figure 33 *IR PL spectra from a C-implanted and annealed porous Si sample measured from room-temperature to 10K.*

5 CONCLUSIONS

Phase I results demonstrated for the first time a strong, stable blue-green photoluminescence from C-implanted red-emitting porous Si using photoexcitation. Catholuminescence measurements performed at the University of Colorado show blue and orange emission at 1.80 eV and 2.80 eV. The objective of Phase I was to obtain blue-green emission from porous silicon structures either by increasing the bandgap of the substrate by growth of Si-C random alloys prior to forming nanostructures with quantum confined properties, or by increasing the confinement energy of red-emitting Si nanostructures.

Porous Si structures fabricated on epitaxially-grown Si-C random alloys showed a 1 to 2 order of magnitude increase in the intensity of red light emission compared to that from porous Si fabricated on non-epitaxial Si. However, a significant blue shift was observed after carbon implantation into red-emitting porous Si (non-epitaxial) substrates. This blue-green emission was observable by the naked eye. Using $Al_{0.30}Ga_{0.70}As$ as a reference, we observed that the intensity of the green-blue emission was much higher than that of the original red-emitting porous Si.

The electron diffraction pattern of C-implanted and annealed bulk Si has confirmed the formation of β-SiC, which has a bandgap of 2.2 eV. Fourier transform infrared (FTIR) spectra of green-blue emitting porous structures shows infrared absorption lines identical to that of SiC. Electron diffraction studies of blue-green light-emitting porous structures clearly show reflections corresponding to β-SiC. Based on our present experimental data: (1) blue-green emission in PL measurements; (2) blue and orange emission in catholuminescence measurements; (3) presence of a SiC phase by electron diffraction studies; (4) presence of a SiC absorption line in FTIR measurements, we conclude that blue-green light is from SiC nanostructures with quantum confined properties. This material may be used to fabricate blue light emitting Si-based devices which can be easily integrated into Si technology.

In Phase II, in addition to the optimization process we will fabricate blue-green light emitting devices based on p-type SiC nanostructures and ECR deposited GaN. GaN and SiC are both lattice matched, oxygen-free materials and therefore, we expect very strong blue-green emission from GaN/SiC (nanostructure) devices.

6 REFERENCES

1. W. Michaelis and M.H. Pilkuhn, *Phys. Stat. Sol.* **36**, 311 (1969).
2. K. Zweibel, Harnessing Solar Power, (Plenum Press, New York and London, 1990).
3. H. Rupprecht, J.M. Woodall, K. Konnerth, and D.G. Pettit, Appl. Phys. Lett., **9**, 221 (1966).
4. T.P. Lee and A.G. Dentai, IEEE J. Quantum Electron., **14**, 150 (1978).
5. L.T. Canham, *Appl. Phys. Lett.* **57**, 1046 (1990).
6. M.I.J. Beale, N.G. chew, M.J. Uren, A.G. Cullis, and J.D. Benjamin, Appl. Phys. Lett., **46**, 86 (1985).
7. Y.H. Yie, W.L. Wilson, F.M. Ross, J.A. Muncha, and E.A. Fitzgerald, *Mat. Res. Soc. Symp. Proc.*, Boston, MA, Dec. 2-6, 1991.
8. T. van Buren, Y. Gao, T. Tiedje, J.R. Dahn, B.M. Way, *Appl. Phys. Lett.* **60**, 3013 (1992).
9. V. Lehmann and U. Goesele, Appl. Phys. Lett. **58**, 856 (1991).
10. C.H. Perry, F. Lu, F. Namavar, N.M. Kalkhoran, R.A. Soref, *Appl. Phys. Lett.* **60**, 3117 (1992).
11. F. Namavar, H.P. Maruska, and N.M. Kalkhoran, Appl. Phys. Lett., **60**, 2514 (1992).
12. H.P. Maruska, F. Namavar, and N.M. Kalkhoran, Appl. Phys. Lett. **61** (11) (1992).
13. A. Richter, W. Lang, P. Steiner, F. Lozlowski, and H. Sandmeier, Mat. Res. Soc. Symp. Proc., **246**, 209 (1991).
14. N. Koshida and M. Katsuno, Appl. Phys. Lett., **60**, 347 (1992).
15. F. Namavar, N.M. Kalkhoran, and H.P. Maruska, U.S. Patent No. 5,272,355 (December 21, 1993).
16. N.M. Kalkhoran, F. Namavar, and H.P. Maruska, in Light Emission from Silicon, eds. S.S. Iyer, L.T. Canham, and R.P. Collins, (MRS Pittsburg, PA 1992), **256**, 23.
17. H.P. Maruska, F. Namavar, and N. Kalkhoran, Appl. Phys. Lett., **63**, (45) 1993.
18. H.P. Maruska, F. Namavar, and N.M. Kalkhoran, Mat. Res. Soc. Symp., **283** 383 (1993).
19. F. Namavar, R.F. Pinizzotto, H. Yang, N. Kalkhoran, P. Maruska, Mat. Res. Soc. Symp. Proc., **298**, 343 (1993).
20. N.M. Kalkhoran, Mat. Res. Soc. Symp. Proc., **283**, 365, (1993).
21. N.M. Kalkhoran, F. Namavar, H.P. Maruska, Appl. Phys. Lett., **63**, 2661 (1993).
22. J.P. Proot, C. Delerue, and G. Allan, Appl. Phys. Lett., **61**, 1948 (1992).
23. B.S. Meyerson, private communication, 1991.
24. R.A. Soref, *J. Appl. Phys.*, **72**, 4736 (1992).
25. S.S. Iyer, K. Elbert, M.S. Goorsky, F.K. Legoues, F. Cardone, and B.A. Ek, Mat. Res. Soc. Proc. **220**, 581 (1991).
26. W.E. Hoke, P.J. Lemonias, D.G. Weir, H.T. Hendriks, and G.S. Jackson, J. Appl. Phys. **69**, 513 (1991).
27. J.A. Borders, S.T. Picraux, and W. Beezhold, Appl. Phys. Lett., **18**, 509 (1973).
28. J.A. Baker, T.N. Tucker, N.E. Moyer, and R.C. Buschert, J. Appl. Phys., **39**, 4365 (1968).
29. T. Matsumoto, J. Takahashi, T. Tamaki, T. Futagi, H. Mimura, and Y. Kanemitsu, Appl. Phys. Lett., **64**, 2 (1994).

DISTRIBUTION

Office of Naval Research
Scientific Officer
Attn: Guy Beaghler
NCCOSC RDTE DIV (NRaD)
53570 Silvergate Avenue, Room 2070
San Diego, CA 92152-5070

DCMAO Boston
Attn: Robert Muldoon
495 Summer Street
Boston, MA 02210-2138

Director, Naval Research Laboratory
ATTN: Code 2627
Washington, DC 20375

Defense Technical Information Center
Building 5, Cameron Station
Alexandria, VA 22304-6145

Department of Defense
Ballistic Missile Defense Organization
ATTN: T/IS
7100 Defense Pentagon
Washington, DC 20301-7100